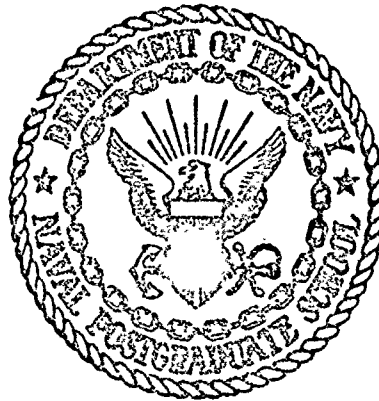


FR
P

NAVAL POSTGRADUATE SCHOOL

Monterey, California

ADA 025672



THESIS

AN EXPERIMENTAL INVESTIGATION OF THE
WHISTLER NOZZLE AND AN ANALYTICAL
INVESTIGATION OF A RING WING IN
SUPERSONIC FLOW

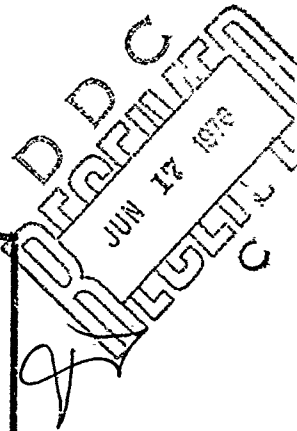
by

Donald L. Weiss
March 1976

Thesis Advisor:

M. F. Platzler

Approved for public release; distribution unlimited.



Unclassified

SECURITY CLASSIFICATION OF THIS PAGE (When Data Entered)

REPORT DOCUMENTATION PAGE

READ INSTRUCTIONS BEFORE COMPLETING FORM

1. REPORT NUMBER		2. GOVT ACCESSION NO.		3. RECIPIENT'S CATALOG NUMBER	
4. TITLE (and Subtitle)		5. TYPE OF REPORT & PERIOD COVERED			
AN EXPERIMENTAL INVESTIGATION OF THE WHISTLER NOZZLE AND AN ANALYTICAL INVESTIGATION OF A RING WING IN SUPERSONIC FLOW		Master's Thesis, March 1976			
6. AUTHOR		6. PERFORMING ORG. REPORT NUMBER			
Donald L. Weiss		8. CONTRACT OR GRANT NUMBER(s)			
9. PERFORMING ORGANIZATION NAME AND ADDRESS		10. PROGRAM ELEMENT, PROJECT, TASK AREA & WORK UNIT NUMBERS			
Naval Postgraduate School Monterey, California 93940					
11. CONTROLLING OFFICE NAME AND ADDRESS		12. REPORT DATE		13. NUMBER OF PAGES	
Naval Postgraduate School Monterey, California 93940		Mar 1976		96	
14. MONITORING AGENCY NAME & ADDRESS (if different from Controlling Office)		15. SECURITY CLASS. (of this report)			
Naval Postgraduate School Monterey, California 93940		Unclassified			
16. DISTRIBUTION STATEMENT (of this Report)		15a. DECLASSIFICATION/DOWNGRADING SCHEDULE			
Approved for public release; distribution unlimited.					
17. DISTRIBUTION STATEMENT (of the abstract entered in Block 20, if different from Report)					
18. SUPPLEMENTARY NOTES					
19. KEY WORDS (Continue on reverse side if necessary and identify by block number)					
Ring Wing, Whistler Nozzle, Entrainment, Thrust Augmentation					
20. ABSTRACT (Continue on reverse side if necessary and identify by block number)					
This thesis consists of two parts. First, an experimental investigation of a new device called the whistler nozzle was conducted. Experiments were conducted in the areas of nozzle efficiency, mass entrainment, and flow visualization. Flow visualization showed the presence of a Coanda type jet wall interaction in the nozzle collar. Thrust efficiencies indicated that whistling could be achieved without much greater losses					

6

10

11

12 96p.

next page

061450

Unclassified

SECURITY CLASSIFICATION OF THIS PAGE(When Data Entered)

20.

→ than the basic axisymmetric jet. Entrainment tests were inconclusive regarding the whistler nozzle performance. Second, supersonic flow past an oscillating cylindrical shell is analyzed using linearized characteristics methods. Pressure distributions and generalized aerodynamic forces are calculated and presented for various radius to length ratios and reduced frequencies. Good agreement is obtained in the two dimensional limiting case with previous work by Platzer, and an early solution of the steady cylindrical case by Zierep. ↖

ACCESSION for	
NTIS	White Section <input checked="" type="checkbox"/>
DTIC	Buff Section <input type="checkbox"/>
UNCLASSIFIED	<input type="checkbox"/>
JUSTIFICATION	
BY	
DISTRIBUTION/AVAILABILITY CODES	
REG.	MAIL. TAG. or SPECIAL
A	

Unclassified

SECURITY CLASSIFICATION OF THIS PAGE(When Data Entered)

AN EXPERIMENTAL INVESTIGATION OF THE WHISTLER NOZZLE AND
AN ANALYTICAL INVESTIGATION OF A RING WING IN SUPERSONIC
FLOW

by

Donald L. Weiss
Second Lieutenant, USMC
B.S.A.E., USNA, 1974

Submitted in partial fulfillment of the
requirements for the degree of

MASTER OF SCIENCE IN AERONAUTICAL ENGINEERING

from the
NAVAL POSTGRADUATE SCHOOL
March 1976

Author:

Donald L. Weiss

Approved by:

Max F. Phelan

Thesis Advisor

Daniel F. Collins

Second Reader

Richard W. Lee

Chairman, Department of Aeronautics

J. P. ...

Academic Dean

ABSTRACT

This thesis consists of two parts. First, an experimental investigation of a new device called the whistler nozzle was conducted. Experiments were conducted in the areas of nozzle efficiency, mass entrainment, and flow visualization. Flow visualization showed the presence of a Coanda type jet wall interaction in the nozzle collar. Thrust efficiencies indicated that whistling could be achieved without much greater losses than the basic axisymmetric jet. Entrainment tests were inconclusive regarding the whistler nozzle performance. Second, supersonic flow past an oscillating cylindrical shell is analyzed using linearized characteristics methods. Pressure distributions and generalized aerodynamic forces are calculated and presented for various radius to length ratios and reduced frequencies. Good agreement is obtained in the two-dimensional limiting case with previous work by Platzler, and an early solution of the steady cylindrical case by Zierep.

TABLE OF CONTENTS

LIST OF FIGURES.....	6
ACKNOWLEDGEMENT.....	8
I. INTRODUCTION-THE WHISTLER NOZZLE.....	9
II. RELATED PAST WORK.....	12
III. SCOPE OF RESEARCH.....	18
IV. NOZZLE DESCRIPTION.....	19
V. DESCRIPTION OF EXPERIMENTS.....	21
A. THRUST EFFICIENCIES.....	21
B. MASS ENTRAINMENT.....	24
C. FLOW VISUALIZATION.....	32
VI. RESULTS AND DISCUSSION.....	36
VII. CONCLUSIONS AND RECOMMENDATIONS.....	45
VIII. INTRODUCTION- THE RING WING.....	46
IX. PROBLEM FORMULATION.....	47
X. METHOD OF CHARACTERISTICS.....	52
XI. GENERALIZED AERODYNAMIC FORCE.....	55
XII. RESULTS AND DISCUSSION.....	57
XIII. CONCLUSIONS AND RECOMMENDATIONS.....	66
APPENDIX A ISENTROPIC THRUST CALCULATIONS.....	67
APPENDIX B ENTRAINMENT RATIO CALCULATIONS.....	68
APPENDIX C ENTRAINMENT CHAMBER DESIGN.....	70
APPENDIX D PROGRAM LISTINGS AND DOCUMENTATION.....	74
LIST OF REFERENCES.....	94
INITIAL DISTRIBUTION LIST.....	96

LIST OF FIGURES

1.	Whistler Nozzle Cross Section.....	11
2.	Various Whistler Configurations.....	13
3.	Coanda Effect.....	16
4.	Whistler Nozzle and Plenum.....	20
5.	Thrust Bed.....	22
6.	Thrust Bed Calibration Curve.....	23
7.	Experimental Thrust Curve.....	25
8.	Entrainment Chamber Cutaway View.....	28
9.	The entrainment Chamber and Peripheral Gear.....	29
10.	Orifice Pressure Difference vs Entrainment Ratio....	31
11.	Tuft Ring Photo.....	34
12.	Lampblack Pooling Illustration.....	35
13.	Thrust Efficiency Results.....	38
14.	Entrainment Ratio Results and Comparison Data.....	39
15.	Entrainment Ratio vs Reynolds Number.....	40
16.	Tuft Pictures, Results.....	43
17.	Ring Wing Illustration.....	48
18.	Axial Pressure Distribution, 2D Limiting Case.....	58
19.	Axial Pressure Distribution, Comparison With Zierep.	59
20.	Numerical Instability Illustration.....	61

21. Pitching Moment vs Reduced Frequency.....	63
22. Pitching Moment vs Outer Radius To Length Ratio.....	64
23. Representative Axial Pressure Distribution, Including One Reflection.....	65

ACKNOWLEDGEMENT

I wish to express my great appreciation to Mr. Stan Johnson for his invaluable help and advice throughout the course of this thesis project. I would also like to thank Mr. Ron Ramaker for the excellent work he did in constructing the entrainment chamber, a primary part of this work. Finally, I would like to thank Professor M. F. Platzer whose advice and direction were a great help, and Connie, my wife, without whose help this thesis might never have been written and typed.

I. INTRODUCTION-THE WHISTLER NOZZLE

The phenomenon of entrainment is a process through which a moving fluid increases its mass flow, by "grabbing up" the medium it is flowing in. The moving fluid is called the working fluid, and might be the primary water jet in an ejector pump. The medium might be any other fluid, say oil, in the case of the ejector pump.

The entrainment process has found practical use for quite a long time. Analytical descriptions of the entrainment process exist; however, none is general enough to describe all cases of practical interest. Even the relatively simple case of a steady jet in still air is rather difficult because of the many configurations which one would like to describe. Thus interest and research in this area continues, perhaps with more intensity than previously due to the recent interest in new V/STOL configurations which would employ this process. One such is the Navy's XFV-12A, which is expected to derive a large amount of thrust through the augmentation, or entrainment, of its primary thrust using wing mounted ejectors.

The success of concepts such as the augments wing depends on many factors, an important one being the rate of entrainment of the primary jet, and another being its efficiency. This rate of entrainment is the rate of increase of jet mass flow with axial distance away from the jet nozzle. The rate of entrainment and nozzle efficiency are characteristics which vary with nozzle configuration.

As mentioned earlier, there is a large variety of steady nozzle configurations. Lobe, slot, and hypermixing

nozzles are some which have drawn recent interest for their entrainment capabilities. One should not neglect unsteady nozzle configurations, however, as such effects as swirling the primary flow, and oscillating the primary flow in a bi-stable manner (fluidic oscillator), also show promise in their ability to entrain.

One of the newest nozzle configurations to surface is an unsteady nozzle. Perhaps the simplest in construction of all unsteady nozzles, it is illustrated in figure 1. The whistler nozzle, as it is called, produces a loud pure tone while in operation. Additionally, it creates a relatively large rate of entrainment. It is the whistler nozzle which is the subject of this thesis.

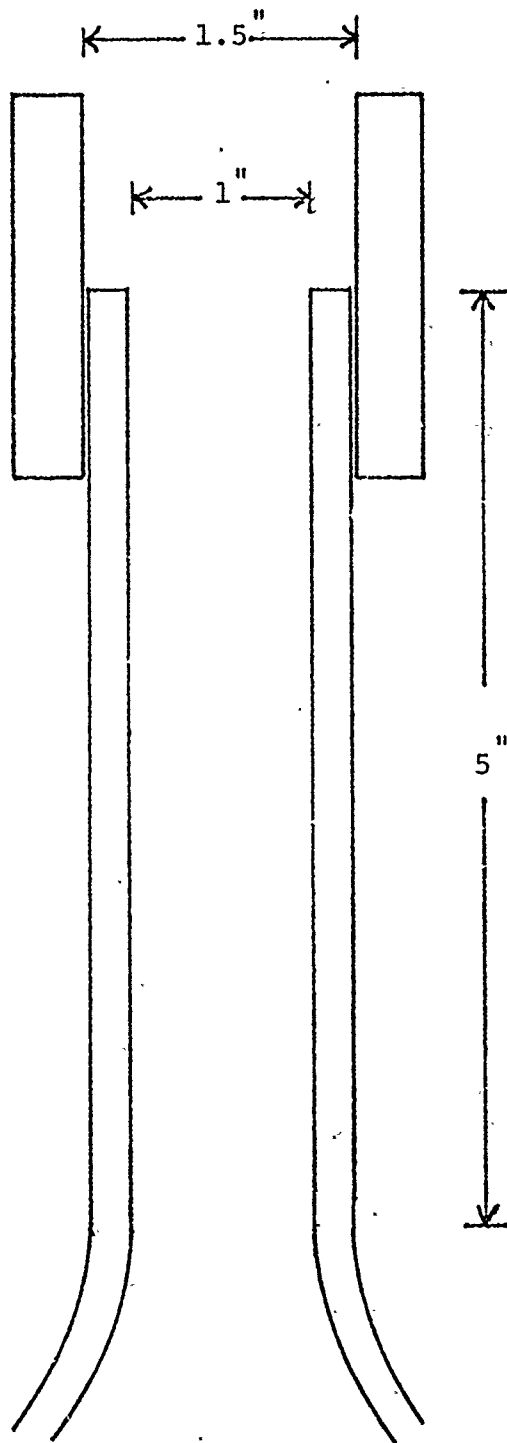


Figure 1 - WHISTLER NOZZLE CROSS SECTION

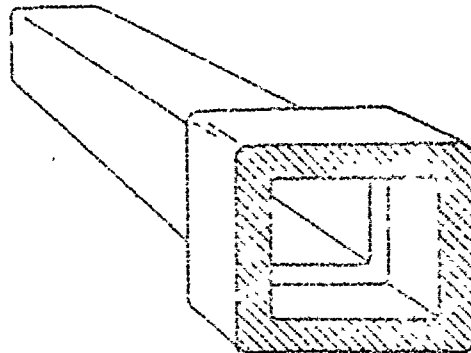
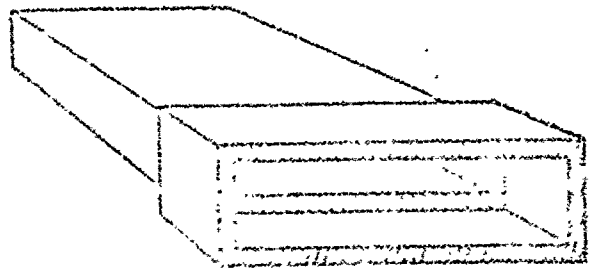
II. RELATED PAST WORK

The earliest work done on the whistler nozzle was by Hill and Greene (reference 1). In 1974, they cited the discovery of a new phenomenon, characteristic of a new device which they named the whistler nozzle. Their basic configuration, as illustrated in figure 1, consisted of a convergent section, followed by a section of constant area followed by a step change in cross sectional area to another section of constant area. The length of the last section could be varied to produce loud pure tones of varying frequency, through the excitation of a standing acoustic wave in the final section, much as in an organ pipe. Hill and Greene observed that the whistler produced a greatly increased mixing rate, and decided that this was due to acoustic stimulation of the jet. Increased mixing rate of an axisymmetric jet due to acoustic stimulation is a process that had been observed earlier by Crow and Champagne (reference 5).

In addition to the basic axisymmetric configuration, many other configurations were found to produce the whistling phenomenon. A few are illustrated in figure 2. Common to all of these was that the step in cross section had to extend completely around the jet. Also noted was the apparent presence of a separation reattachment cycle, occurring at the nozzle lip:

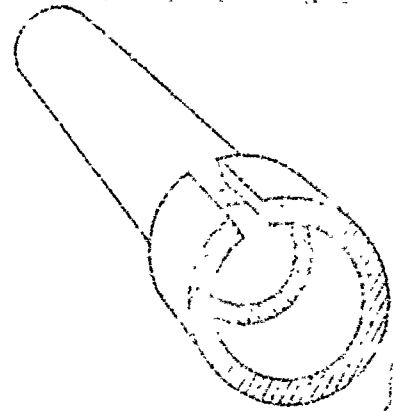
No further study seems to have been performed concerning the whistler nozzle, save a report in 1975 by Hill and Jenkins (reference 2), in which they reestablished the operating characteristics of the nozzle, and its ability to entrain more air.

Rectangular Whistler



Square Whistler with rounded corners

Split Collar Whistler



Elliptical Exit Contour Whistler

Figure 2 - VARIOUS WHISTLER CONFIGURATIONS

Hill and Greene's work has been summarized, since their original report, in comprehensive reviews of the ejector state of the art by Schum (reference 3), and by Viets (reference 4). These reports call attention to the whistler nozzle's promise in rate of entrainment, and the lack of data regarding the whistler thrust efficiency.

Although no further research directly involving the whistler is available, much work has been done in the area of free jets, and entrainment, which might prove valuable in a study of the whistler nozzle.

An obviously important area of related work is the sensitivity of free jets to acoustic stimulation. Probably the best known and most definitive work in this area was performed by Crow and Champagne (reference 5). By mounting a speaker inside the plenum chamber they managed to excite a free axisymmetric jet, at various frequencies. The effect of the sound was to produce a velocity fluctuation in the nozzle exit plane. It was observed that the turbulent structure of the jet was sensitive to the acoustic excitation. Through the use of high-speed schlieren photography it was observed that under acoustic stimulation the turbulent structure of the jet developed a large-scale vortex structure, as contrasted with the small scale vortex sheet surrounding a normal jet. Attendant to the formation of the large-scale vortices, an increase in the mixing rate was also observed.

Others, such as Bevilacqua and Lykoudis (reference 6), have observed the turbulent structure in steady, free jets. The presence of a large-scale vortex structure has been observed in such jets at low Reynolds numbers. It appears that the large-scale structure disappears as Reynolds number increases. However, according to the findings of

Crow and Champagne, it may be reexcited through acoustic stimulation. It may be conjectured from experimental evidence that the entrainment process is a combination of a large-scale "scooping up" of the ambient fluid, and a small-scale nibbling away at the ambient fluid. These entrainment processes would correspond to the large and small scale vortex structures around a free jet.

A further area of related research, perhaps not obvious, is the well known Coanda effect. The basic whistler configuration sets up a flow situation somewhat akin to that of a bistable fluidic element, or fluidic oscillator. The difference between the two cases is that the fluidic oscillator oscillates between two positions, while the whistler must oscillate between many circumferential positions. That such an oscillation takes place seems indicated by the nozzle configuration and the separation reattachment cycle noted by Hill and Greene.

Reference 10 provides a good summary of the mechanism of the Coanda effect, as well as its characteristics regarding reattachment and sensitivity to sound. Though the following comments relate specifically to two-dimensional flows, it is thought that the general behavior and mechanism should carry over to a three-dimensional situation.

Figure 3 illustrates the Coanda mechanism in two-dimensional flow. As shown, a jet is issuing from an orifice and flowing between two adjacent walls. Because the jet will at some time be nearer to one wall than the other, and because the jet is entraining air, a pressure difference across the jet will develop that pulls the jet to the closer wall. This attachment forms a region of circulating flow. The point of jet attachment is determined by this region, in which a balance is struck between flow entrained by the jet and flow reinjected by the jet.

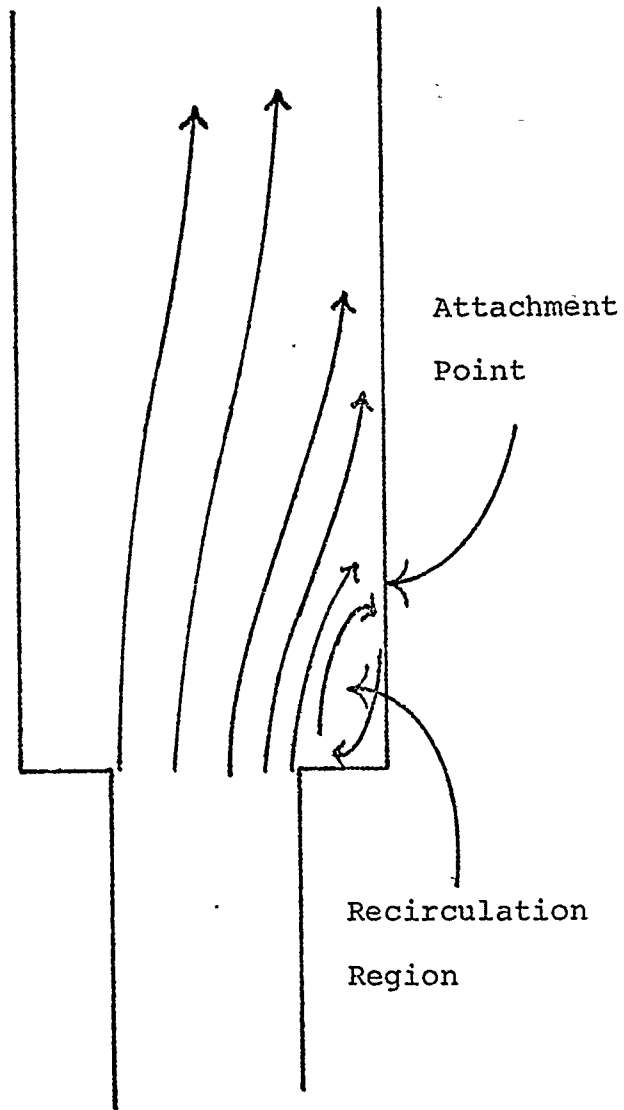


Figure 3 - COANDA EFFECT

Anything that disrupts this balance causes the attachment point of the jet to shift.

Observation has shown that the attachment point in Coanda effect is sensitive to jet velocity and sound, within a range of Reynolds numbers. In the range of Reynolds number from 200 to 3000, under the effect of increasing jet velocity, or a sound input of increasing amplitude, the attachment point has been observed to move upstream. This upstream movement appears to approach a limiting position, beyond which the point will not move.

Reference 10 relates the effects of jet velocity and sound on the attachment point to the point of transition from laminar to turbulent flow of the jet. Both increasing jet velocity and a sound input will move the transition point closer to the jet exit. This movement will increase the length of turbulent flow across the recirculation region. A turbulent jet entrains more air than a laminar jet, and thus the balance of flow in the recirculation region is disrupted, with a resulting upstream move of the attachment point.

III. SCOPE OF RESEARCH

The intent of this research was to provide a clearer insight into the workings of the whistler nozzle, and to develop an improved understanding of the ways in which one may effect control over the characteristics of a free jet.

Specific areas of research were the nozzle thrust efficiency, the nozzle entrainment rate, and visualization of the lip interaction process described by Hill and Greene. Accordingly, experiments were conducted to obtain relevant data. Thrusts were measured on a thrust bed, mass entrainment measured in a device patterned after that developed by Ricou and Spalding (reference 7), and high speed motion pictures taken of tufts about the nozzle lip.

IV. NOZZLE DESCRIPTION

The whistler nozzle used in all tests is illustrated in figure 4. It consisted of a small plenum, convergent section, short constant area section and a moveable collar over the constant area section. The inner whistler diameter was 1 inch, while the collar diameter was 1.5 inches. The nozzle configuration was essentially that used by Hill and Greene in their investigations. The characteristic dimension used for Reynolds number and nondimensionalization of axial distance from the nozzle was the inner nozzle diameter, 1 inch.

Whistler
Nozzle

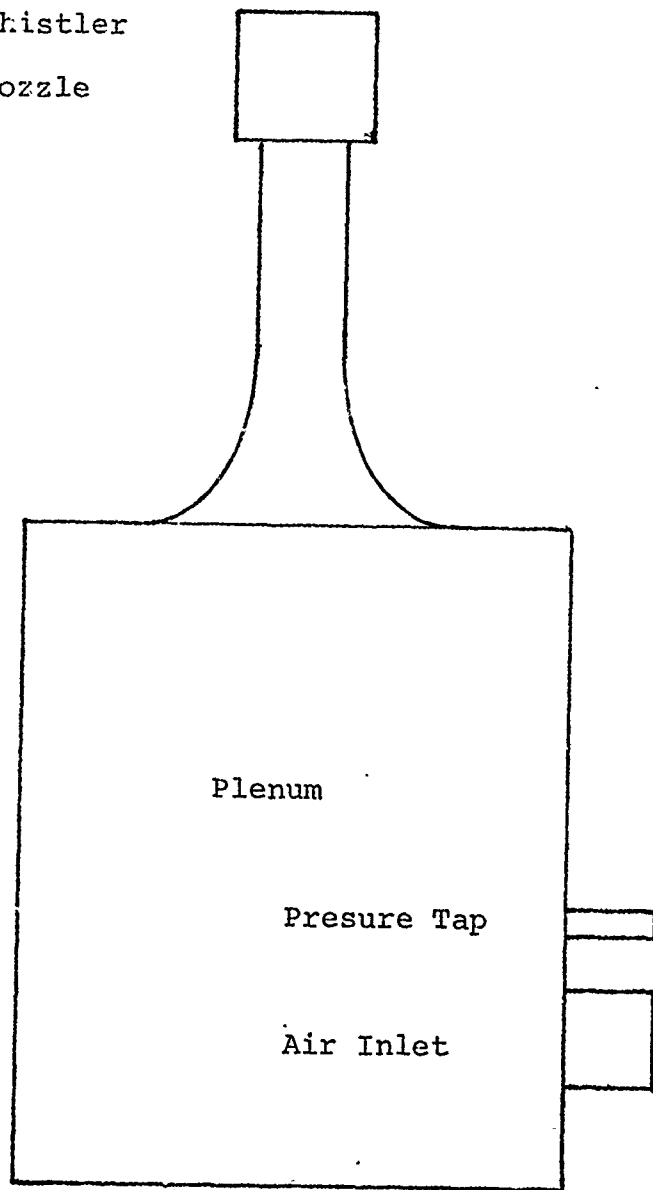


Figure 4 - WHISTLER NOZZLE AND PLENUM

V. DESCRIPTION OF EXPERIMENTS

A. THRUST EFFICIENCIES

Thrust efficiencies were obtained by measuring nozzle thrust. A comparison was made between measured and calculated thrust.

Test equipment consisted of a thrust bed and the nozzle. The thrust bed was configured to measure horizontal thrust, and slid on two tracks, mounted to a solid foundation. The nozzle plenum was clamped to the thrust bed which was in turn secured to the foundation through a load ring, mounted with a load cell, the device that actually measured thrust. Air was supplied to the nozzle from a large tank, connected to the plenum through a regulator and a flexible tube which led vertically away from the plenum, so as not to bias the thrust measurements in any way. Calibration was performed with the use of a tray, connected to the bed through a cable and pulley arrangement, upon which one placed weights of known magnitude. Peripheral gear required included a voltage source, digital voltage meter, and Wheatstone bridge. Figure 5 illustrates the set up. Plenum pressures were measured using a mercury manometer.

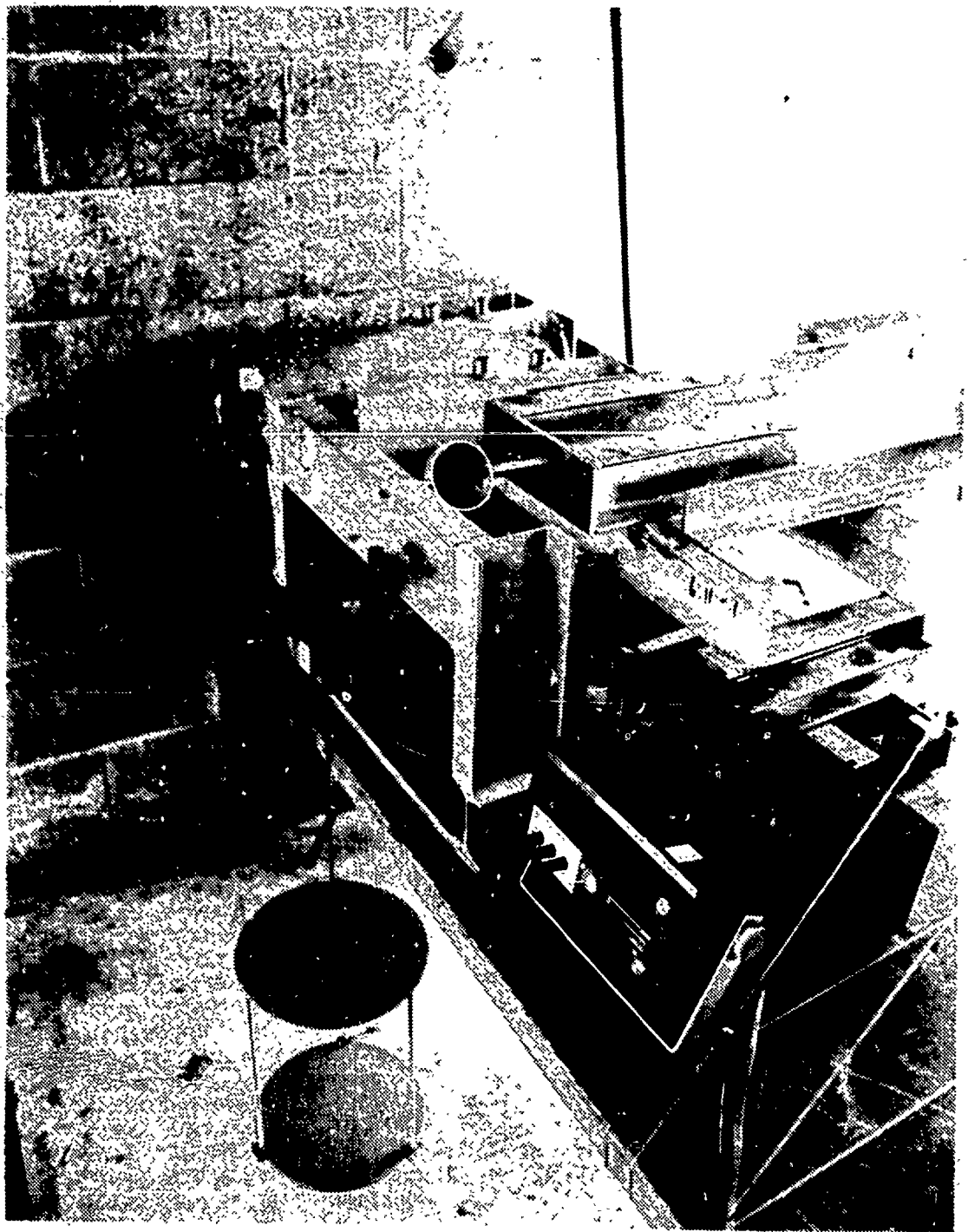


Figure 5 - THPUST BED

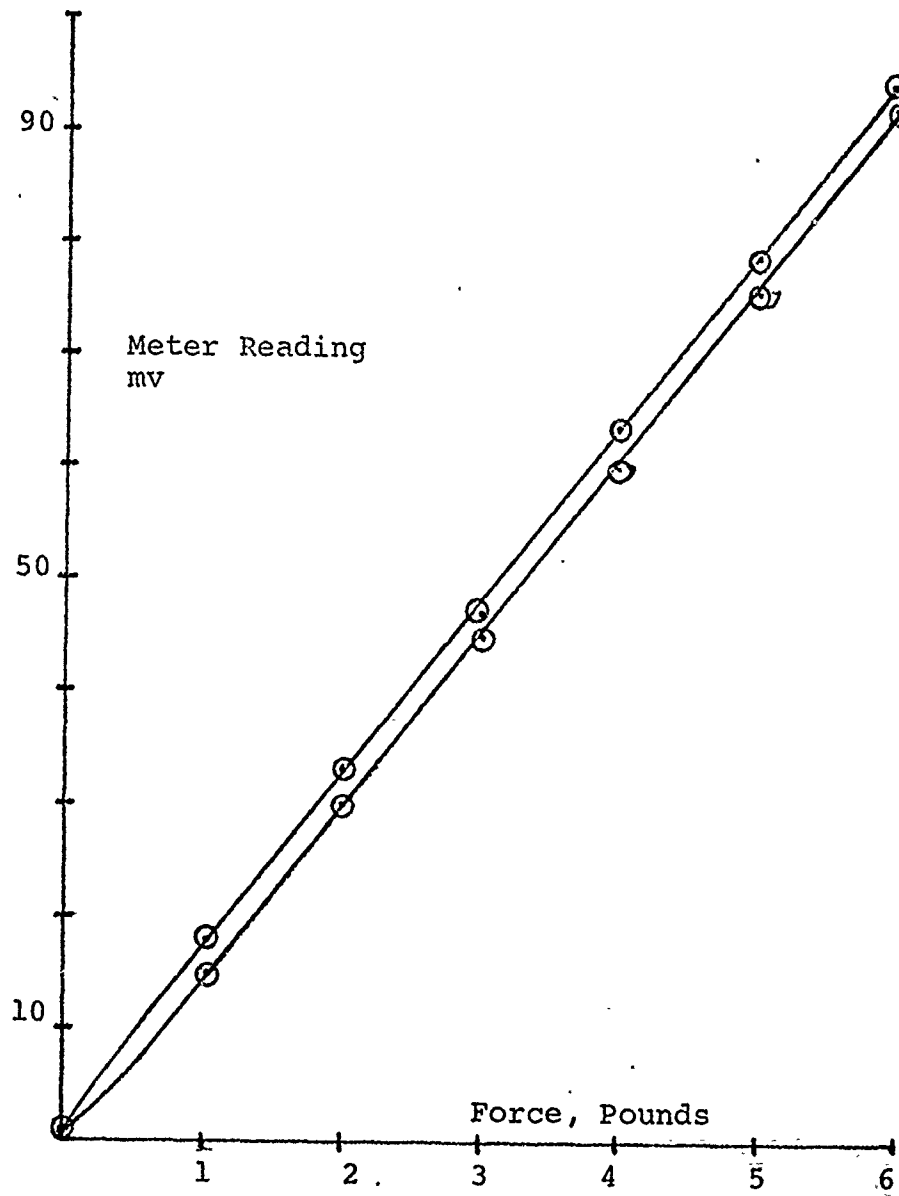


Figure 6 - THRUST BED CALIBRATION CURVE

Calibration of the thrust bed indicated a certain amount of hysteresis in the system, as may be seen in figure 6. Not serious at thrusts of about 6 pounds, it did introduce problems at low thrust levels, and precluded reliable thrust measurement at low Reynolds numbers.

Thrust measurements were made for various collar positions, over a range of nozzle exit velocities. Recorded data included gage pressure in the nozzle plenum, thrust readings from the voltmeter, collar extension, and ambient pressure and temperature.

Measured thrusts were plotted against pressure ratio across the nozzle. Figure 7 presents an example curve. Ideal thrust was calculated according to the procedures in appendix A. Thrust efficiencies were then obtained and plotted against nozzle pressure ratio, exit velocity, and Reynolds number (based on the nozzle diameter).

B. MASS ENTRAINMENT

Mass entrainment was measured directly, using a device patterned after one developed by Ricou and Spalding (reference 7). It was believed that this device should yield more accurate results than an approach using integrated velocity profiles, especially in the case of an unsteady nozzle. Measurements were made at various axial positions, for several collar positions.

The device used will hereafter be referred to as the entrainment chamber. It was designed with the aid of data from a research report by Peschke (reference 8). Appendix B provides a detailed account of the design.

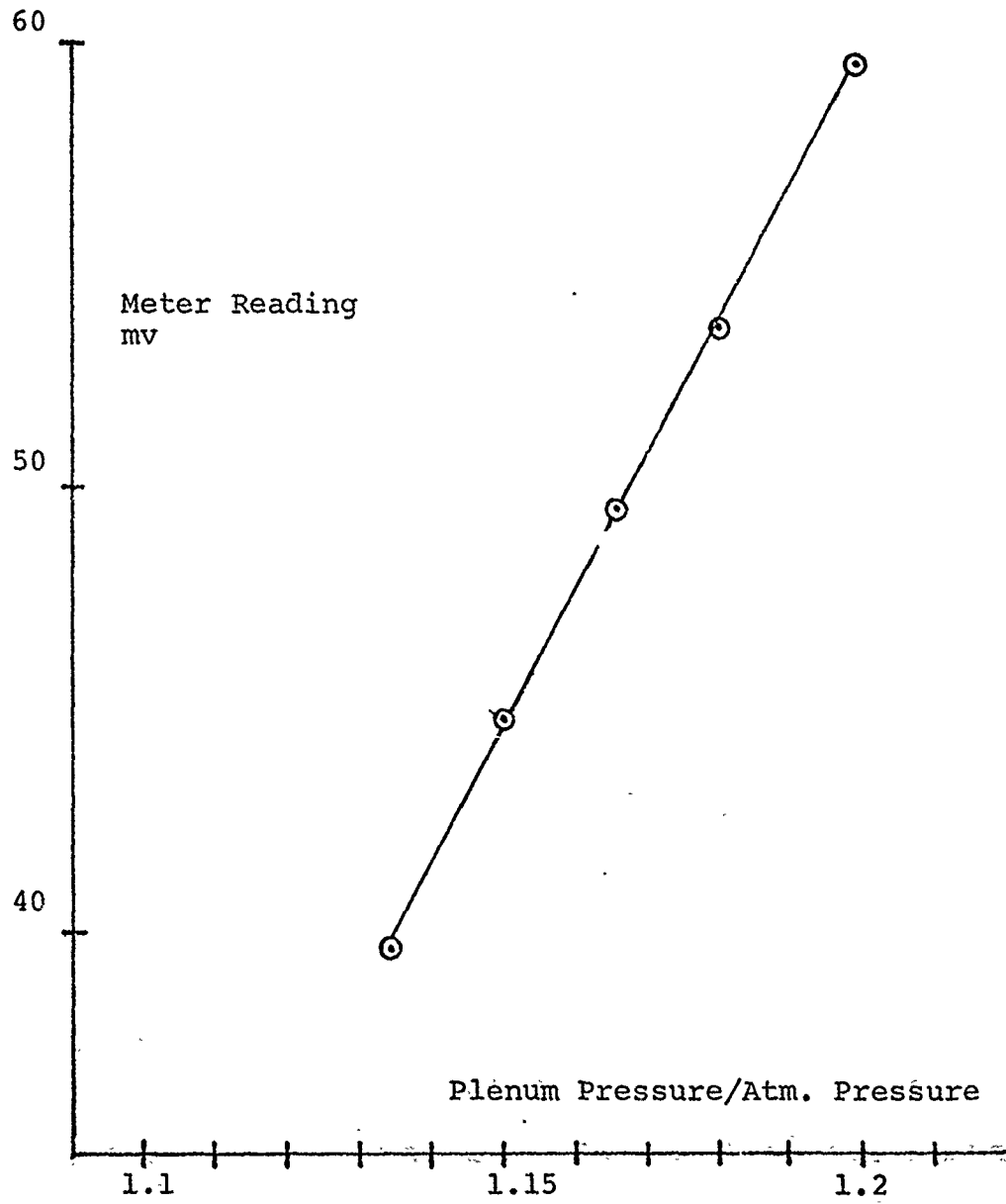


Figure 7 - EXPERIMENTAL THRUST CURVE

The principle of operation is relatively simple. The entrained air of a free jet flows in at a right angle to the jet axis. The entrainment chamber simply blocks this inflow with a circumferential membrane, and seals the ends with a plate at the nozzle and an orifice at the axial station where one wishes to measure the total mass flow. Ideally, all of the entrained air is supplied to the exterior of the membrane from a regulated source. As a free jet does not support any axial pressure gradient, the proper amount of air to supply through the membrane is indicated by the disappearance of any pressure gradient across the orifice. One may regulate the membrane flow to obtain this point. These primary aspects of the device are illustrated in figure 8.

Critical design aspects of the entrainment chamber, especially the orifice sizes, are treated in appendix B. It is sufficient here to simply state that one entrainment chamber was designed to perform measurement of the total jet mass flow at various axial locations.

One primary difference between this chamber's geometry and that of others (references 7 and 8) should be noted. As shown in figure 8, exit orifices were positioned in the porous cylinder at various distances from the nozzle. That portion of the porous cylinder extending above the orifice plate was sealed by a fiberglass cylinder attached to the orifice. Thus, in this situation that portion of the jet beyond the orifice and inside the porous cylinder exit was not in a truly free-jet flow situation. This was as opposed to the reference 7 and 8 configurations where the exit orifice corresponded to the exit of the porous cylinder. Thus, in those experiments the jet past the orifice was in a truly free-jet flow situation. The configuration used in this report was adopted in order to facilitate the measurement of mass flows at many axial locations. It was

hoped that this chamber's geometry would not affect the chamber readings greatly, although some effect was to be expected.

Peripheral equipment to the basic entrainment chamber included flow regulating, metering, and measuring devices. Figure 9 presents a photograph of the chamber and its peripheral gear. Separate air sources, both fed by a large tank, were supplied for the nozzle and membrane. Nozzle flow was metered through an orifice and controlled with a regulator. Because of the much greater mass flow required, membrane air was supplied through a venturi, followed again by a flow regulator. Pressures across the orifice were measured with an inclined water manometer. Pressures across the venturi were measured with a mercury manometer. Pressure across the entrainment chamber orifices was measured with an alcohol micromanometer. Nozzle plenum pressure was measured with a water manometer.

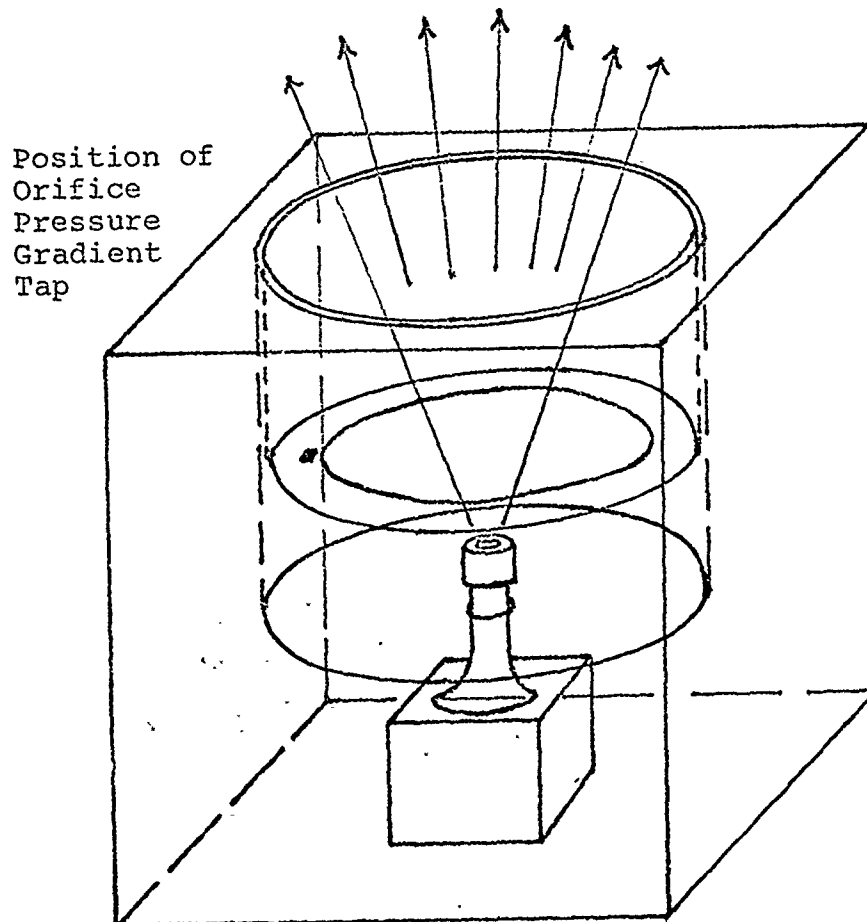
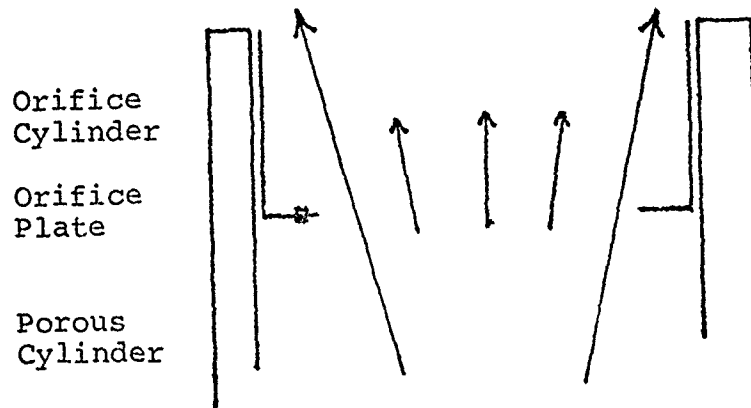


Figure 8 - ENTRAINMENT CHAMBER CUTAWAY VIEW

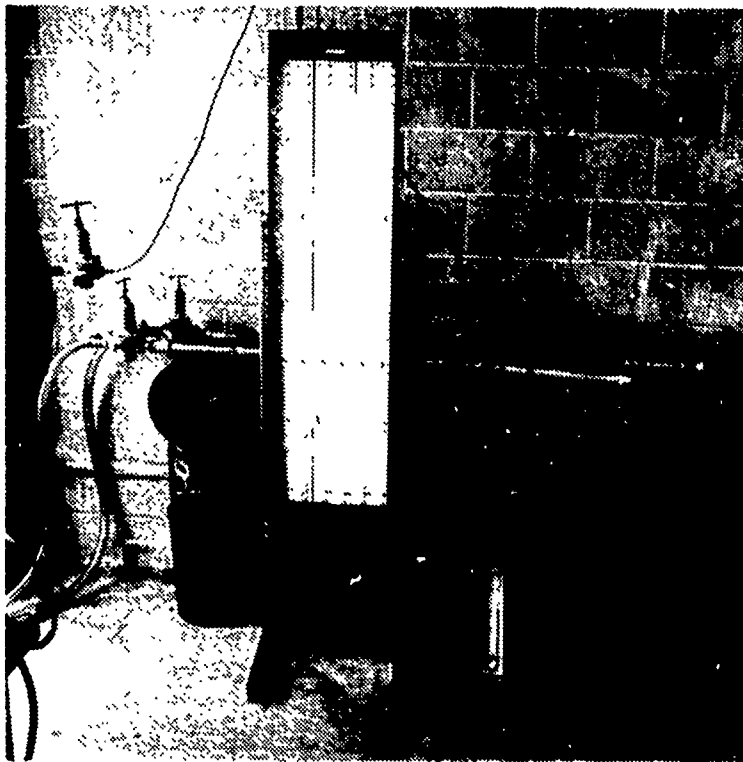


Figure 9 - THE ENTRAINMENT CHAMBER AND PERIPHERAL GEAR

Membrane air temperature was measured just after the venturi, using a mercury thermometer.

Entrainment measurements were made at various axial locations for various collar positions. Recorded data included pressure difference across the venturi and orifice, pressure difference across the entrainment chamber orifice, nozzle plenum pressure, ambient pressure, air temperature in the membrane supply, and collar position. Standard procedure for each run was to vary the membrane airflow so that one obtained both positive and negative pressure gradients at the chamber orifice. This provided a more precise location of the proper entrained flow rate. It is of interest to note that, due to hardware limitations and the large amount of air entrained by the jet at the furthest axial locations measured, nozzle exit velocities were limited to around 100 feet per second at the further axial locations. This also affected the number of useful locations for whistler measurements, as a strong whistler oscillation required a relatively large exit velocity, say 300 feet per second.

Data reduction followed standard procedures for the venturi and orifice. These are presented in appendix C. Entrainment was plotted as M/M_0 (total mass flow divided by the primary mass flow), against X/D , axial location divided by nozzle diameter. Working curves of chamber orifice pressure gradient are presented as pressure difference against M/M_0 , in the example plotted in figure 10.

Orifice Pressure Gradient
Inches of Manometric Fluid

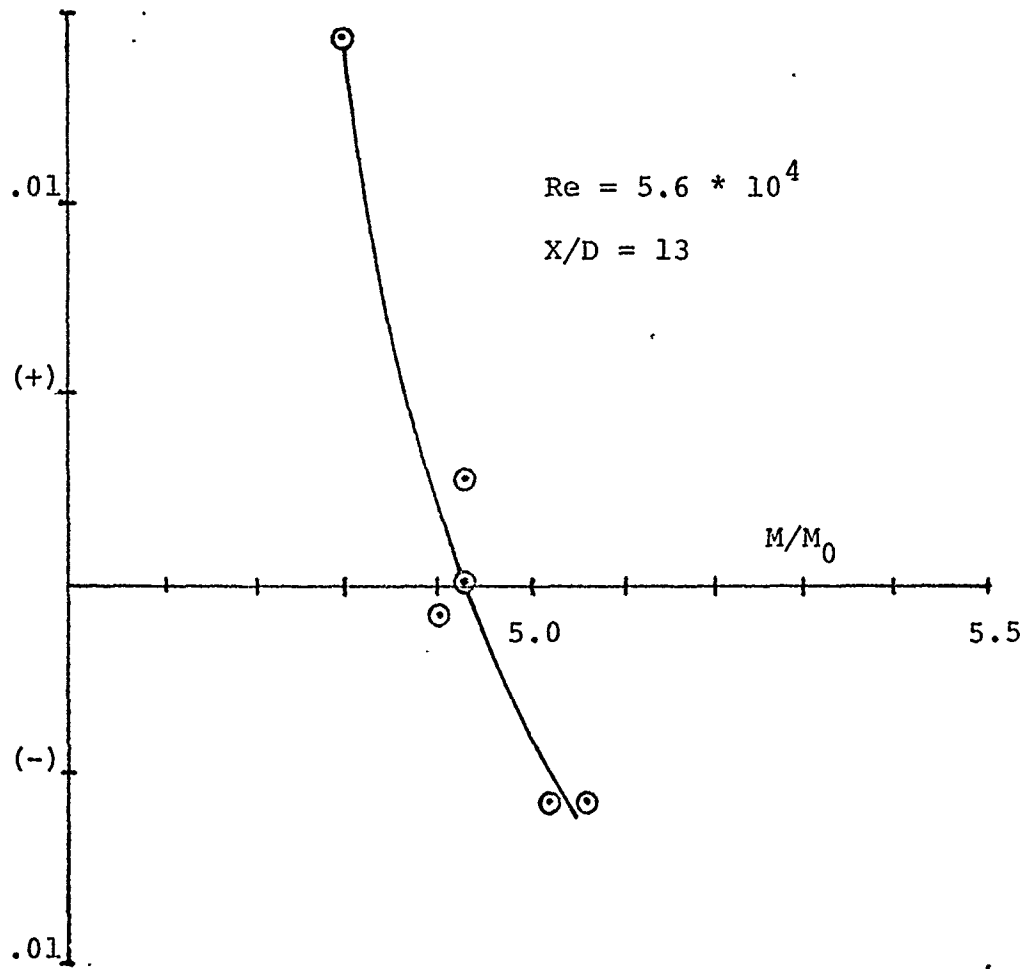


Figure 10 - ORIFICE PRESSURE DIFFERENCE VS ENTRAINMENT RATIO

C. FLOW VISUALIZATION

Flow visualization of the nozzle jet lip interaction was performed in two ways: high-speed motion photography of a ring of tufts at the nozzle lip, for the purpose of discerning a pattern to the interactions; and a mixture of lamp black and kerosene inside the nozzle collar in order to observe the behavior of the separation reattachment location.

Photographic equipment consisted of a Honeywell Pentax single reflex camera, a Bolex Supreme handheld 16mm movie camera, and a Redlake Hycam 16mm high-speed movie camera. The tuft ring was simply constructed of cotton threads held by a masking tape ring, and a photo of the ring is presented in figure 11. Observation in the lampblack experiment was performed with the naked eye and no peripheral equipment was necessary.

Photographic tests were to be done in three phases. High-speed still shots were first taken to determine the usefulness of the tufts for visualization, and to obtain the approximate required film speed for motion photography. Next, medium speed motion pictures, 64 frames per second, were taken to confirm the necessity of the high-speed camera. Finally, high-speed motion pictures were taken to visually control the tuft motion such that useful observations could be made. No particular collar settings or exit velocities were used in photographic work. The only requirement was to produce the oscillation phenomenon, which was never difficult. As it turned out, a lack of time prevented the completion of the high-speed photography phase.

Lampblack tests were performed in two ways. The inside of the collar extension was liberally coated with the lampblack mixture, and either exit velocity varied at constant collar setting, or collar setting varied at constant exit velocity. Observations were all visual, none quantitative, save noting the range of exit velocities covered, which was from about 100 to 300 feet per second. The lampblack mixture was observed to pool as illustrated in figure 12, and the downstream-most edge of the pool was interpreted as indicating the location on the collar of reattachment and separation.



Figure 11 - TUFT RING PHOTO

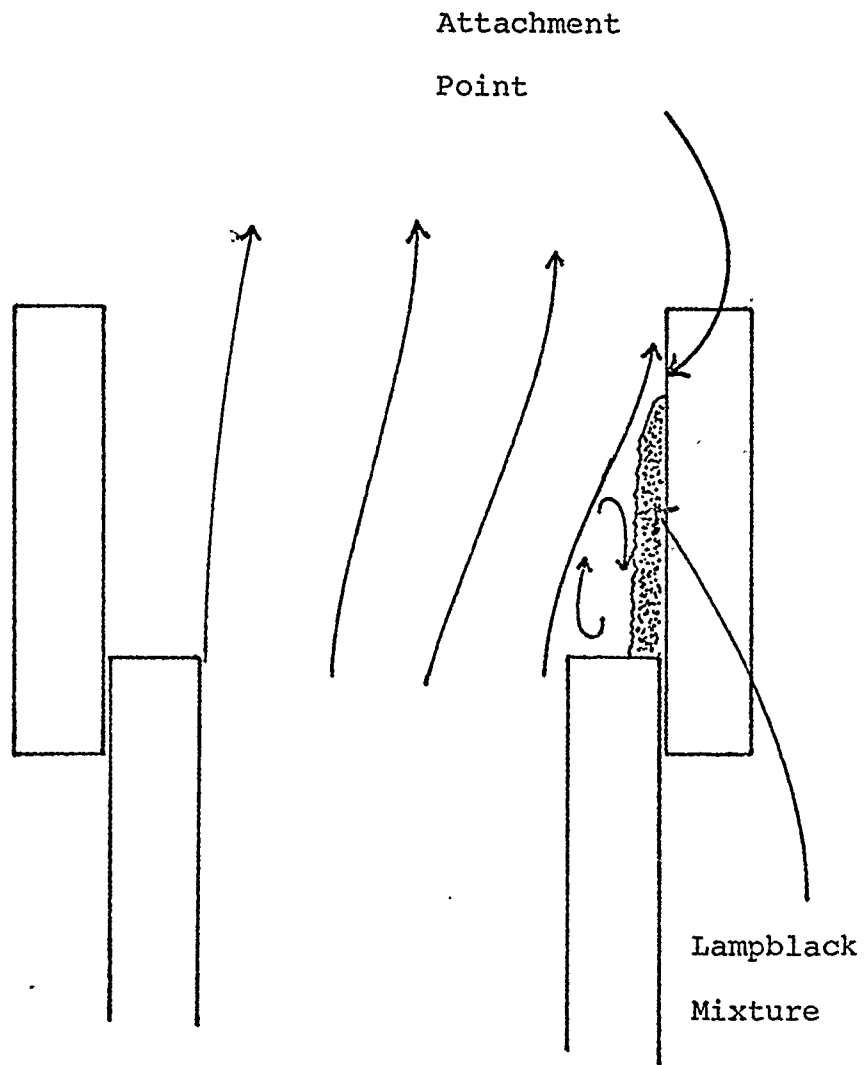


Figure 12 - LAMPBLACK POOLING ILLUSTRATION

VI. RESULTS AND DISCUSSION

Nozzle thrust efficiency results are presented in figure 13, plotted for various collar positions. The whistler oscillation was produced at each collar setting for the whole range of Reynolds numbers shown, although sudden frequency jumps did occur in this range. These frequency jumps did not appear to change the nozzle thrust or thrust efficiency in any discontinuous manner. Instead the trend was as indicated, progressively decreasing nozzle efficiency with increasing collar extension. The zero collar extension efficiencies were found to be about 6 percent lower than those found in a previous report (reference 8). This is believed due to the extremely simple, unflared configuration of the nozzle, which may be seen in figure 4. Reference 8 nozzles were divergent nozzles and as such should be more efficient. Important to note is that the whistler oscillations may be obtained without much reduction in the basic nozzle efficiency.

Entrainment results are presented in figure 14, plotted together with the results of Hill and Greene (reference 1) for comparison. As may be seen, in the case of the basic jet agreement is good qualitatively but poor quantitatively. In the case of the whistler nozzle agreement is not good in any way. It is believed that the poor quantitative comparison was due to interference of the deep orifice cylinders with the jet. These create a pressure gradient from the orifice to the chamber exit which quite possibly affects the readings. As noted in the experiment section, and in Appendix C, these orifice cylinders constitute a major difference in configuration

from the chambers of reference 7 and 8. Additionally, in the case of the whistler nozzle, it is believed the method of enclosing the jet up to the axial position of measurement may interfere with the sound - jet interaction (especially the cloth porous cylinder) and the formation of a large-scale turbulent structure. Figure 15 illustrates that readings taken were relatively constant with Reynolds number. As noted by Ricou and Spalding, the entrainment ratio can be a strong function of Reynolds number in certain ranges of Reynolds number. It is interesting to note that this behavior is supported by the present notion of jet turbulence structure and its development as exit velocity increases, which postulates that the major contributor to entrainment, the large scale structure, disappears as Reynolds number increases.

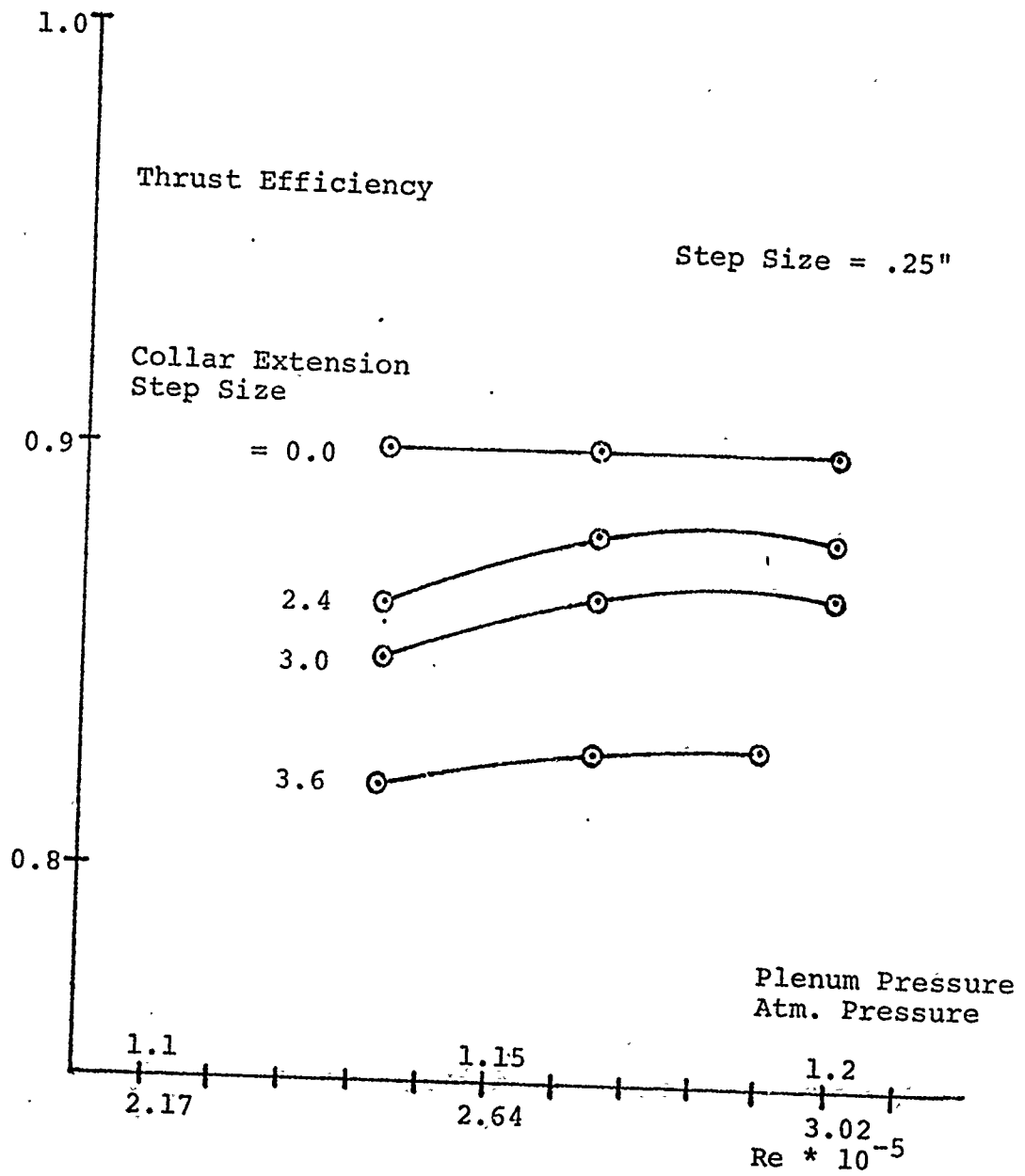


Figure 13 - THRUST EFFICIENCY RESULTS

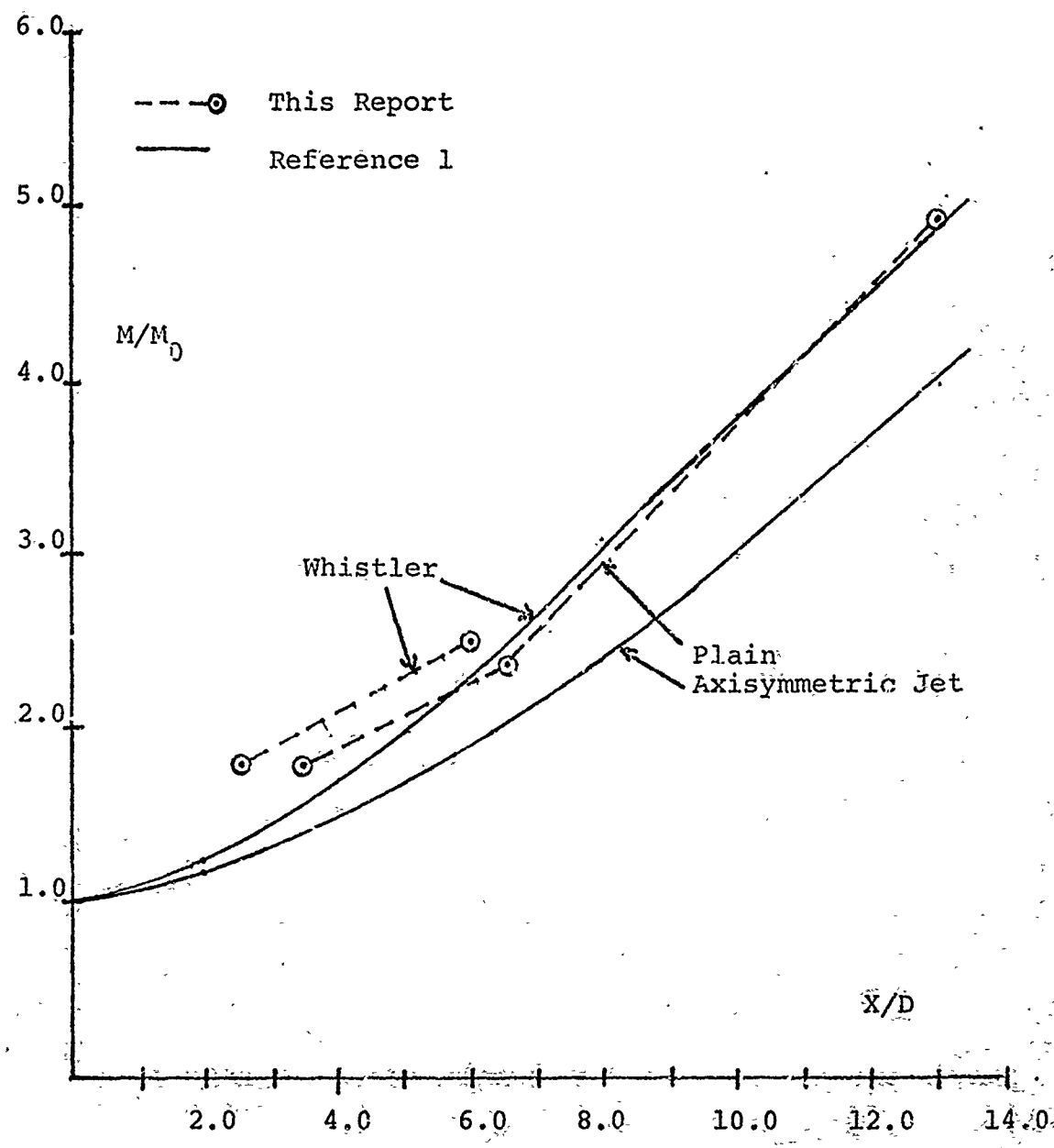


Figure 14 - ENTRAINMENT RATIO RESULTS AND COMPARISON DATA

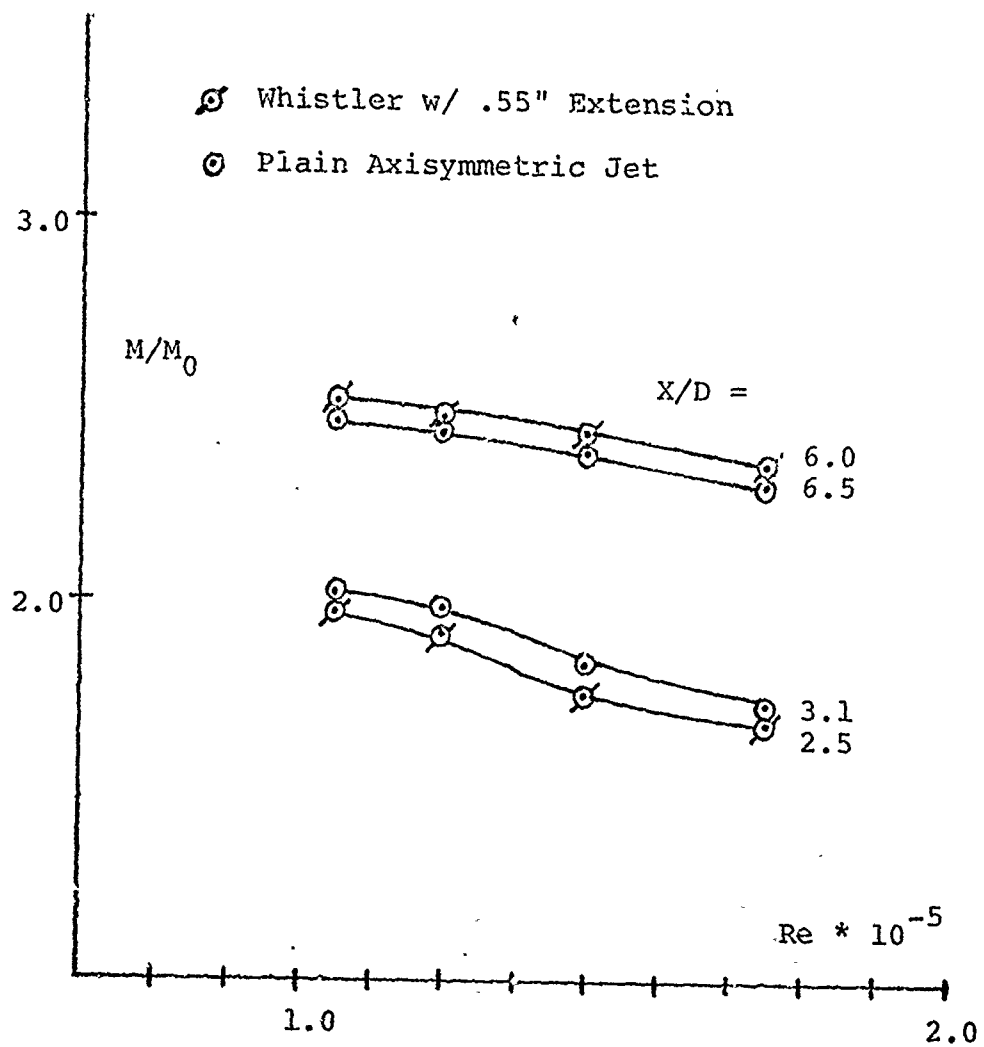


Figure 15 - ENTRAINMENT RATIO VS REYNOLDS NUMBER

Lack of time precluded testing at more jet axial locations, as each location required a different orifice cylinder (see appendix A). Of the original four orifice cylinders constructed using reference 8 data, only two were useable as the spreading angles encountered averaged about 28 degrees, or 10 degrees less than those used in reference 8. In order to be effective, the orifices had to be positioned at axial distances further than they were designed for. One of those was modified to obtain readings at its design position, also. The larger two were never effective. Another problem encountered was the mass flow limitation of the porous cylinder air supply. This restricted the useable nozzle flow at axial locations beyond X/D of about 6 to such low values that a whistler oscillation strong enough to affect the entrainment could not be produced.

It was hoped that high speed motion pictures would be taken of the tuft experiment; however, this phase of the photographic experiments was not reached. The effectiveness of the tufts in indicating the circumferential collar positions of attached and detached flow was proven in the high-speed still picture phase. Motion pictures with a 64 frame per second camera showed that a much higher speed camera was necessary to slow the motion such that motion pictures would be useful in slowing the tuft motion to a reasonable speed. The necessary film speed was estimated as about 800 frames per second; however, the pictures were never taken. Some representative still pictures are presented in figure 16.

Lampblack tests appeared to be productive as indicators of the general behavior of the collar attachment point. Indications are that a sort of Coanda effect is involved, modified by the fact that while the jet is attached at any

point on the collar there are other points where detached flow allows a backflow into the collar jet gap, which tends to relieve the Coanda effect causing a circumferential shift in the point (or points) of attachment. At a fixed collar extension, with increasing jet velocity, the attachment point was observed to move upstream to a limiting position, just as the Coanda jet described in reference 10. However, at fixed exit velocity and increasing collar extension a different behavior was observed. The attachment point seemed to move with the collar until a point was reached at which the frequency of oscillation jumped. At that instant the point of attachment also appeared to jump suddenly back to its original position relative to the jet exit. This behavior indicated some interdependence of the whistler attachment phenomenon and the oscillation phenomenon.

In addition to the above experiments, two other observations were made which verified those of Hill and Greene.

First, it was noted that extension of the whistler collar seemed to increase mass flow through the nozzle.



Figure 16 - TUFT PICTURES, RESULTS

This was confirmed with static pressure measurements in the nozzle 'throat'. These indicated that the collar was acting as an overexpanded diffuser, resulting in an effective exit area slightly greater than the 'throat' cross section but less than the collar cross section, and further resulting in a greater mass flow through the nozzle.

Second, it was noted that a correspondence between frequency of oscillation, jet exit velocity, and collar extension seemed to exist. It was found that by gradually extending the collar as plenum pressure was increased, one could 'follow' a frequency of oscillation. Accordingly, collar extensions were measured and jet velocity calculated at fixed frequencies of oscillation, and it was found that these fixed frequencies corresponded to constant ratios of collar extension to jet velocity, thus confirming the organ pipe character of the whistler oscillation noted by Hill and Greene.

VII. CONCLUSIONS AND RECOMMENDATIONS

The thrust efficiency and mass entrainment characteristics of the whistler nozzle have been measured, in the case of the entrainment, using a technique heretofore not used on an unsteady jet. Further, observations have been made which should contribute to a further understanding of the whistler flow mechanism.

Several directions of further work are indicated. First, it is recommended that a thrust measurement device using a pendulum arrangement, similar to that used in reference 15, be constructed for a more accurate determination of the whistler efficiency. A device of this type might avoid the hysteresis problems encountered with low thrusts on a conventional thrust bed. It is also recommended that a whistler nozzle of smaller throat diameter be constructed to permit mass entrainment measurements, at further jet axial locations, in the entrainment chamber, at the high exit velocities required to produce a strong oscillation. This will also permit further study of the possibility of whistler measurements in the chamber over a greater range of Reynolds number. Next it is recommended that further flow visualization experiments be conducted. Specifically, high speed motion pictures of the tufts used here, and high speed schlieren photography of the jet, should prove useful. Finally, it is recommended that other unsteady nozzles be tested in the chamber, as the poor results obtained here with the whistler are only preliminary and may not be indicative of the usefulness of the chamber with non-acoustic effects such as swirl.

VIII. INTRODUCTION- THE RING WING

The present work concerns a hollow cylinder, axially aligned, in supersonic flow and undergoing small amplitude oscillations in angle of attack. The intent is to calculate the resulting pressure distributions and aerodynamic moments on what might be more properly termed a ring wing.

Previous investigations, i.e. references 12 and 13, have applied the method of characteristics towards the separate calculation of the inner and outer flowfields, as well as pressure distributions and generalized aerodynamic forces, for such a cylinder in supersonic flow whose walls are undergoing small amplitude sinusoidal oscillations, or panel flutter. These previous investigations resulted in computer programs to perform the necessary calculations.

The primary thrust of the present work was the modification of the previously created programs and then the combination of their results to calculate the unsteady pressure distribution, lift and moment on the cylinder undergoing angle of attack oscillations. Finally, using the modified programs, a parametric study of these items was conducted.

IX. PROBLEM FORMULATION

This development is closely based on several previous papers, i.e. references 12 and 13.

Consider a circular cylindrical shell, in supersonic, inviscid, adiabatic flow, whose axis is aligned with the freestream, and which is undergoing small amplitude oscillations in angle of attack, about the Z axis. (figure 17)

The governing equation for this flow situation is the linearized unsteady potential equation, in cylindrical coordinates.

$$(1-M^2) \phi_{xx} + \phi_{rr} + \frac{1}{r} \phi_r + \frac{1}{r^2} \phi_{\theta\theta} - \frac{2M}{c} \phi_{xt} - \frac{1}{c^2} \phi_{tt} = 0$$

The relevant boundary conditions are the flow tangency condition and Sommerfeld's radiation condition, i.e., that disturbances will propagate away from their source.

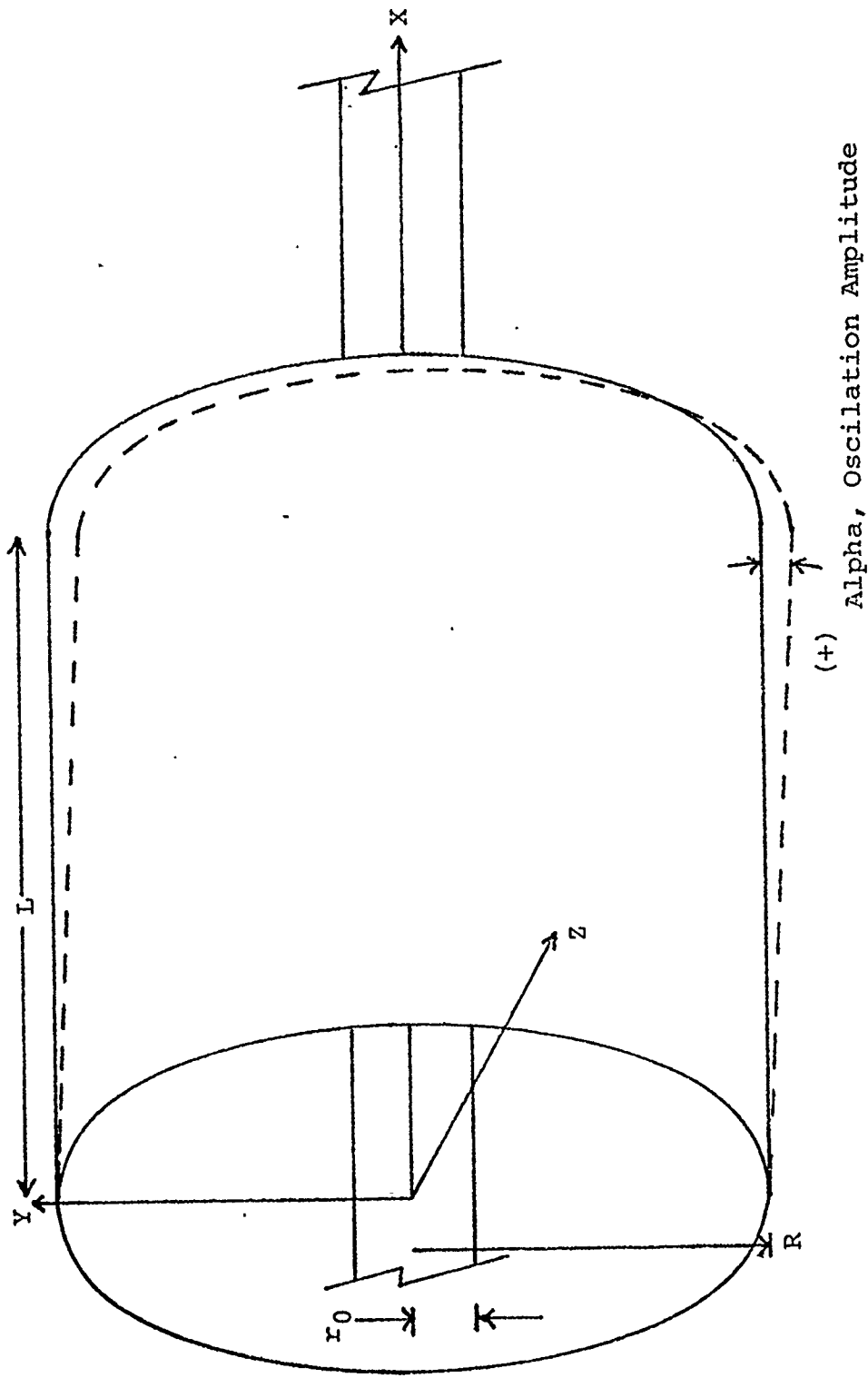


Figure 17 - RING WING ILLUSTRATION

One further condition is necessary, along the X-axis, which amounts to setting the pressure disturbance at the axis equal to zero.

The linearized form of the flow tangency condition is:

$$\left. \frac{\partial \phi}{\partial r} \right|_{r=R} = \frac{\partial h}{\partial t} + U_{\infty} \frac{\partial h}{\partial x}, 0 \leq x \leq L$$

which must be satisfied on the cylinder inner and outer surface.

As stated, the boundary condition at the axis is a zero pressure disturbance:

$$\left. C_p \right|_{r=0} = 0$$

The linearized form of the pressure coefficient is as follows:

$$C_p = \frac{-2}{U_{\infty}^2} \phi_t - \frac{2}{U_{\infty}} \phi_x = \frac{P - P_{\infty}}{q_{\infty}}$$

After nondimensionalization, using cylinder length and length divided by freestream velocity, the above equations become:

$$(1-M^2) \phi_{xx} + \phi_{rr} + \frac{1}{r} \phi_r + \frac{1}{r^2} \phi_{\theta\theta} - 2M^2 \phi_{xt} - M^2 \phi_{tt} = 0$$

$$C_p = -2(\phi_t + \phi_x)$$

subject to:

$$\phi_r \Big|_{r=R} = \frac{\partial h}{\partial t} + \frac{\partial h}{\partial x} \quad , 0 \leq x \leq 1.$$

One now assumes a cylinder oscillation of the form:

$$h(x, \theta, t) = Z(x) \cos(\theta) e^{ikt}$$

where the nondimensional frequency, k , is:

$$k = \frac{\omega l}{U_\infty}$$

The deflection amplitude, $Z(x)$, for the case under consideration, is of the form:

$$Z(x) = \alpha (x - x_0)$$

Following the assumed form of the deflection, the perturbation potential must be of the form:

$$\phi(x,r,\theta,t) = \phi(x,r) \cos(\theta) e^{ikt}$$

and, after substitution, the basic equations become:

$$(1-M^2) \phi_{xx} + \phi_{rr} + \frac{1}{r} \phi_r + \frac{(k^2 M^2 - 1)}{r^2} \phi - i2kM \phi_x = 0$$

$$C_p = -2(\phi_x + ik\phi)$$

subject to:

$$\phi_r \Big|_{r=R} = Z_x + ikZ, \quad 0 \leq x \leq 1.$$

and:

$$C_p \Big|_{r=0} = 0$$

X. METHOD OF CHARACTERISTICS

For supersonic flow, the linearized perturbation potential equation is hyperbolic, and has characteristics which satisfy the following differential equation:

$$(M^2-1) d^2r - d^2x = 0$$

Since the characteristics in supersonic flow correspond to the Mach lines, then for ds , the differential arc length along a characteristic:

$$\frac{dr}{ds} = \pm \frac{1}{M} \quad , \quad \frac{dx}{ds} = \frac{\sqrt{M^2-1}}{M}$$

An arbitrary function, $F(x,r)$, has the following derivatives along the characteristics:

$$\frac{dF}{ds} = F_x \frac{dx}{ds} + F_r \frac{dr}{ds} = \frac{\sqrt{M^2-1}}{M} F_x \pm \frac{1}{M} F_r$$

Defining ds_1 and ds_2 to be the differential arc lengths along the left, and right-running Mach lines respectively, then:

$$F_1 = \frac{dF}{ds_1} \quad , \quad F_2 = \frac{dF}{ds_2}$$

The cross derivatives become:

$$-F_{12} = -F_{21} = \frac{1}{M^2} ((1-M^2) F_{xx} + F_{rr})$$

Solving now for F_x and F_r :

$$F_x = \frac{M}{2\sqrt{M^2-1}} (F_1 + F_2)$$

$$F_r = \frac{M}{2} (F_1 - F_2)$$

Now the basic equations may be written in terms of ϕ and its derivatives along the characteristics as follows:

$$\phi_{12} = \phi_{21} = \frac{1}{2rM} (\phi_1 - \phi_2) + (k^2 - \frac{1}{r^2 M^2}) \phi - \frac{ikM}{M^2-1} (\phi_1 + \phi_2)$$

$$\phi_r = \frac{M}{2} (\phi_1 - \phi_2) = Z_x + ikZ$$

$$C_p = -2(\phi_x + ik\phi)$$

These equations have been put into finite difference form and programmed in Fortran IV for the separate cases of exterior flow and interior flow of a cylinder whose walls were undergoing small amplitude sinusoidal oscillations. In the interior flow program the x axis boundary condition is satisfied on a small inner cylinder in place of the axis, to circumvent problems encountered should r go to zero. For detailed accounts of the equations and programs refer to references 12 and 13.

The primary work here was the transformation of the aforementioned programs to the case under consideration, i.e., a cylinder undergoing small amplitude oscillations in angle of attack, and then a parametric variation study of the pressure distributions and generalized aerodynamic force. The programs were modified such that all cases run were with an angle of attack amplitude of 0.1 radians. Since the basic equation is in a linearized form, the conversion of any results to other angle of attack amplitudes is a simple matter of multiplication. For those interested, the programs resulting from changes required to the reference 12 and 13 programs are listed in appendix D.

XI. GENERALIZED AERODYNAMIC FORCE

As stated above, the results studied were the pressure coefficient amplitude distribution, and the generalized aerodynamic force, Q_{mr} . In its most general form, Q_{mr} is as follows:

$$Q_{mr} = \frac{1}{2} \int C_{pm} \Psi_r(x) dx$$

$$Z(x) = \sum_j A_j \Psi_j(x)$$

where C_{pm} is the pressure coefficient amplitude resulting from the m 'th axial deflection mode, Ψ_r is the r 'th axial deflection mode, and A is the amplitude of the j 'th axial deflection mode. For the special case under consideration, Q takes the following form:

$$Q = \frac{1}{2} \int C_p \Psi(x) dx$$

$$Z(x) = \Psi(x) = \alpha(x - x_0)$$

Thus , in the case under study Q has the special interpretation of being the moment coefficient amplitude about the point X_0 multiplied by the angle of attack amplitude, α , which is equal to 0.1 radians in all cases presented .

XII. RESULTS AND DISCUSSION

Several cases of comparison were considered towards the evaluation of program results. Figure 18 presents two cases of comparison for pressure distributions. The outer radius-to-length ratio was taken to such a value (10) as to approximate a flat plate locally. The inner radius-to-length ratio was taken to such a value (9.75) as to cause a reflection on the inner surface of the outer cylinder.

For sufficiently large radius-to-length ratios the exterior pressure distribution should approximate the theoretical value for a flat plate in supersonic flow, i.e. $2\alpha/\beta$. Figure 18A presents this comparison, and as can be seen agreement is good.

For sufficiently large radius-to-length ratios the interior pressure distribution should approximate the theoretical value for a flat plate. Additionally, if the inner cylinder is of such a radius-to-length ratio as to cause a Mach wave to reflect upon the outer cylinder inner surface, a flow situation exists which should approximate a flat plate in a free jet, where the mach waves are reflected from the jet boundary. This is due to the boundary condition imposed on the inner cylinder, $C_p = 0$. Reference 16 has treated this case in analytic form for small frequencies. Figure 18, A and B, presents a comparison of program results and the results of reference 16. As can be seen agreement is good.

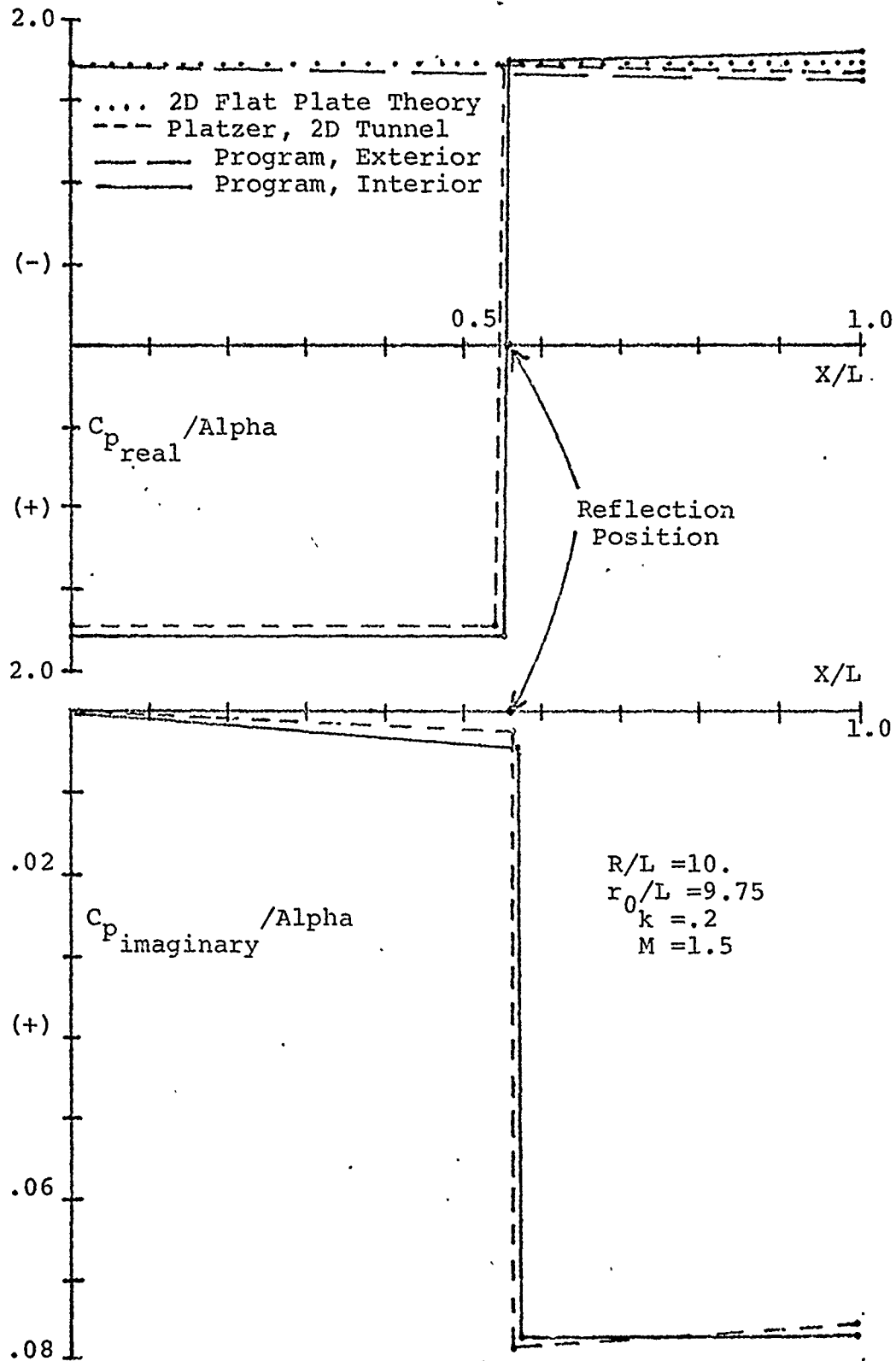


Figure 18 - AXIAL PRESSURE DISTRIBUTION, 2D LIMITING CASE

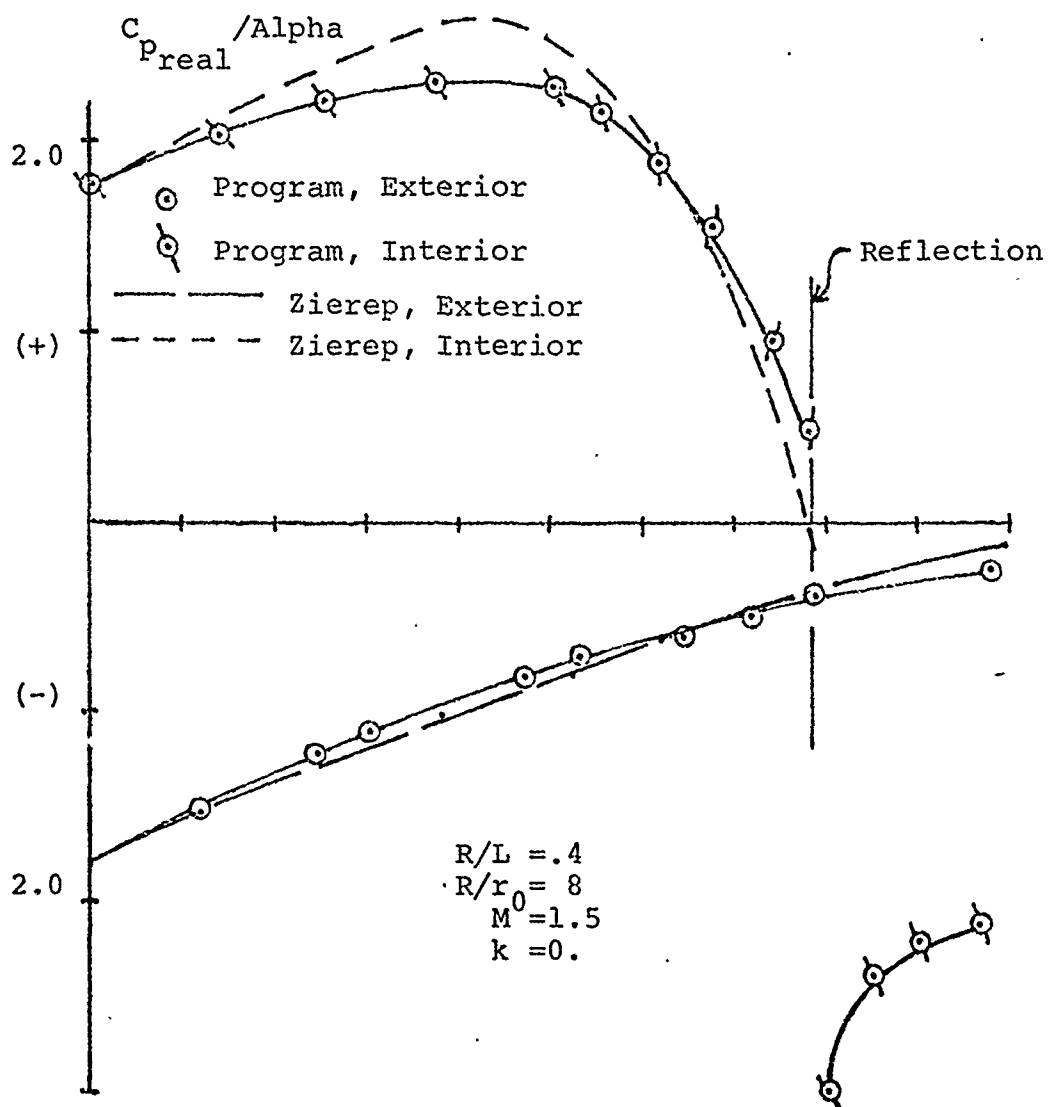


Figure 19 - AXIAL PRESSURE DISTRIBUTION, COMPARISON WITH ZIEREP

Reference 14 has treated the case of a nonoscillating ring wing in supersonic flow. Figure 19 presents a comparison of program results and those of reference 14, for the case shown. As can be seen agreement is fair.

In reference 12, which developed the basic inner flow field program used in this report, the occurrence of a numerical instability in the pressure distributions, under certain conditions, was noted. It was found that this disturbance, which occurred only after a reflection, was due to an undefined constant in the subroutine which computed the boundary condition at the axis. After defining the constant correctly, the pressure distributions were seen to settle down quite nicely. Figure 20 presents a before and after comparison of pressure distributions for a representative case.

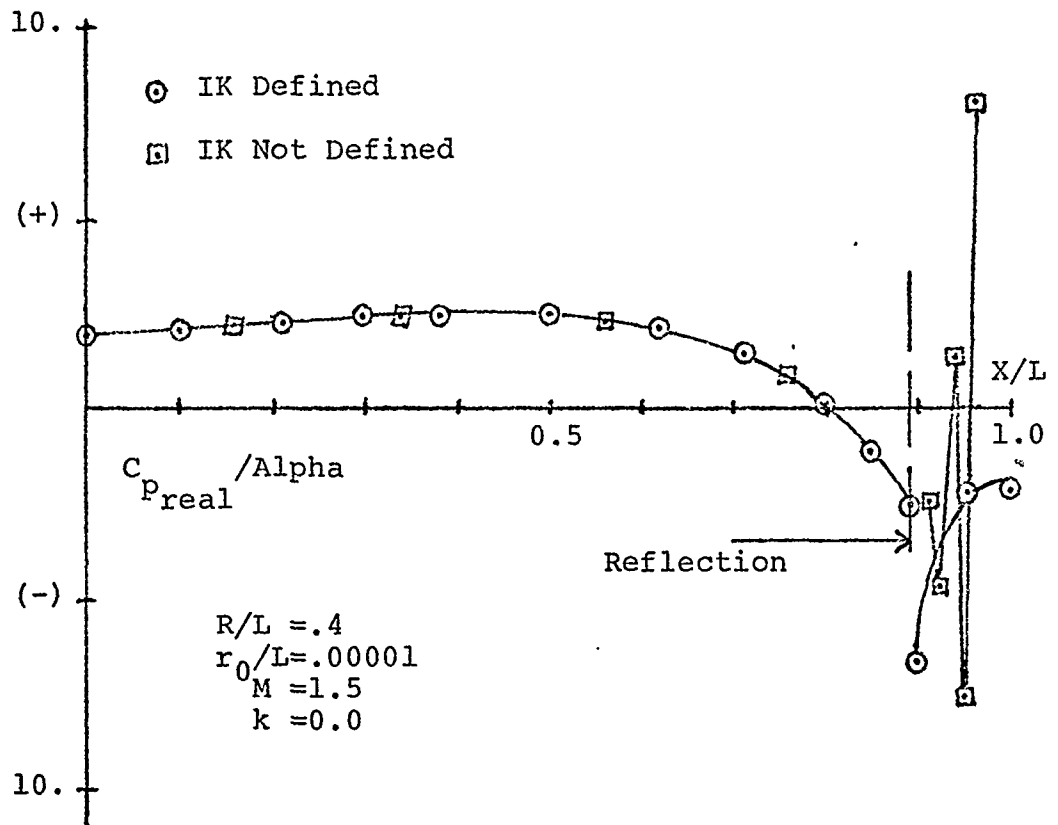


Figure 20 - NUMERICAL INSTABILITY ILLUSTRATION

Figures 21 through 23 present various parametric studies of the moment coefficient, Q , for cases both with and without a reflection on the inner cylinder surface. In these figures the coefficient plotted is actually the difference between that calculated for the inner cylinder surface and that calculated for the outer cylinder surface, divided by the angle of attack amplitude. Thus the coefficients plotted are total moment and pressure coefficients, as opposed to those plotted earlier, which are the coefficients for the inner and outer cases separately. As can be seen from figure 22, for a center of rotation at the leading edge the cylinder has definite geometric regions of stability with respect to angle of attack. Figure 21 illustrates the effect of increased frequency on the moment coefficient. Figure 23 illustrates a typical pressure distribution including one reflection, from which one can infer the reason for the behavior of Q in figure 22, and also the behavior of Q with a varying center of rotation.

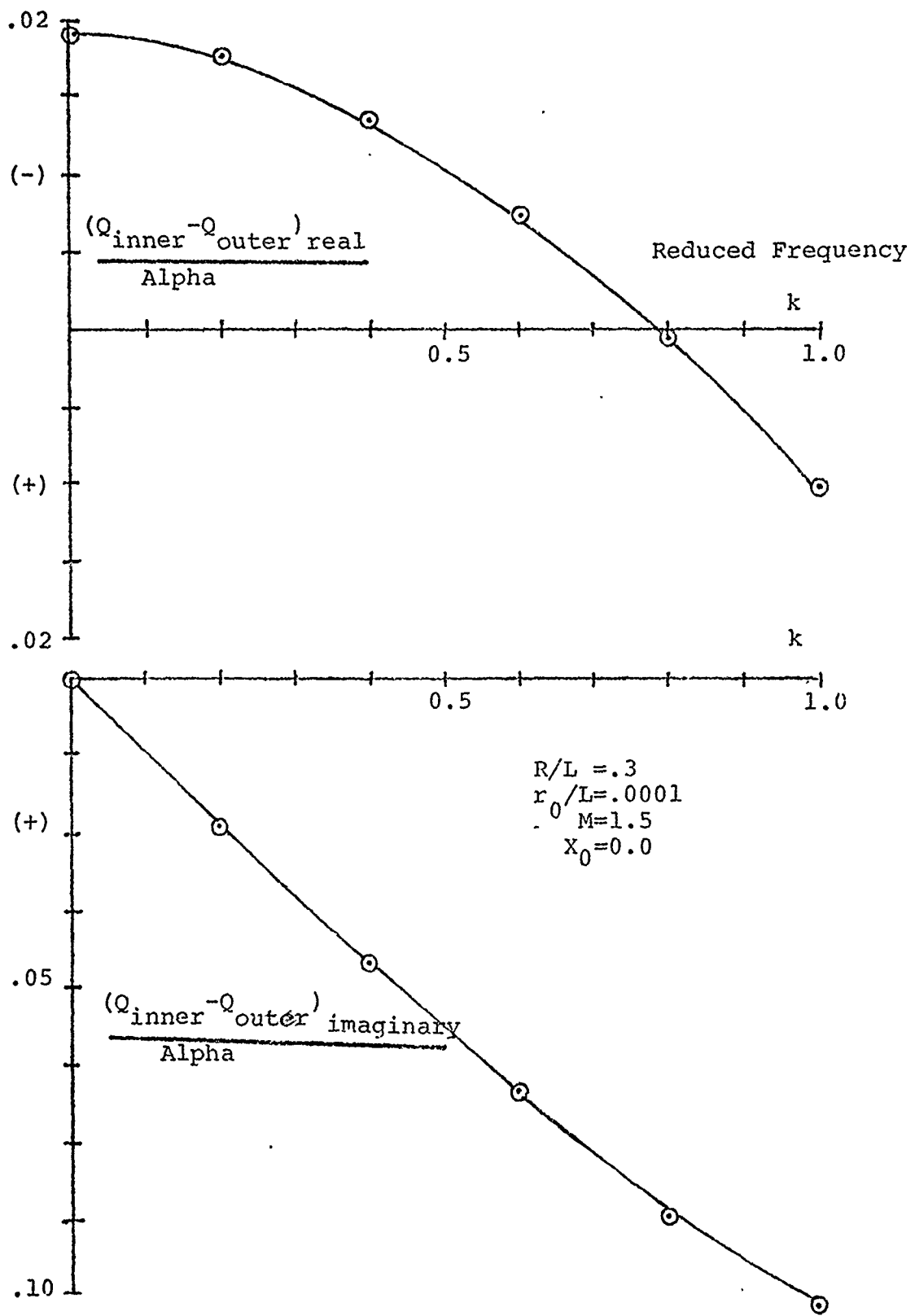


Figure 21 - PITCHING MOMENT VS REDUCED FREQUENCY

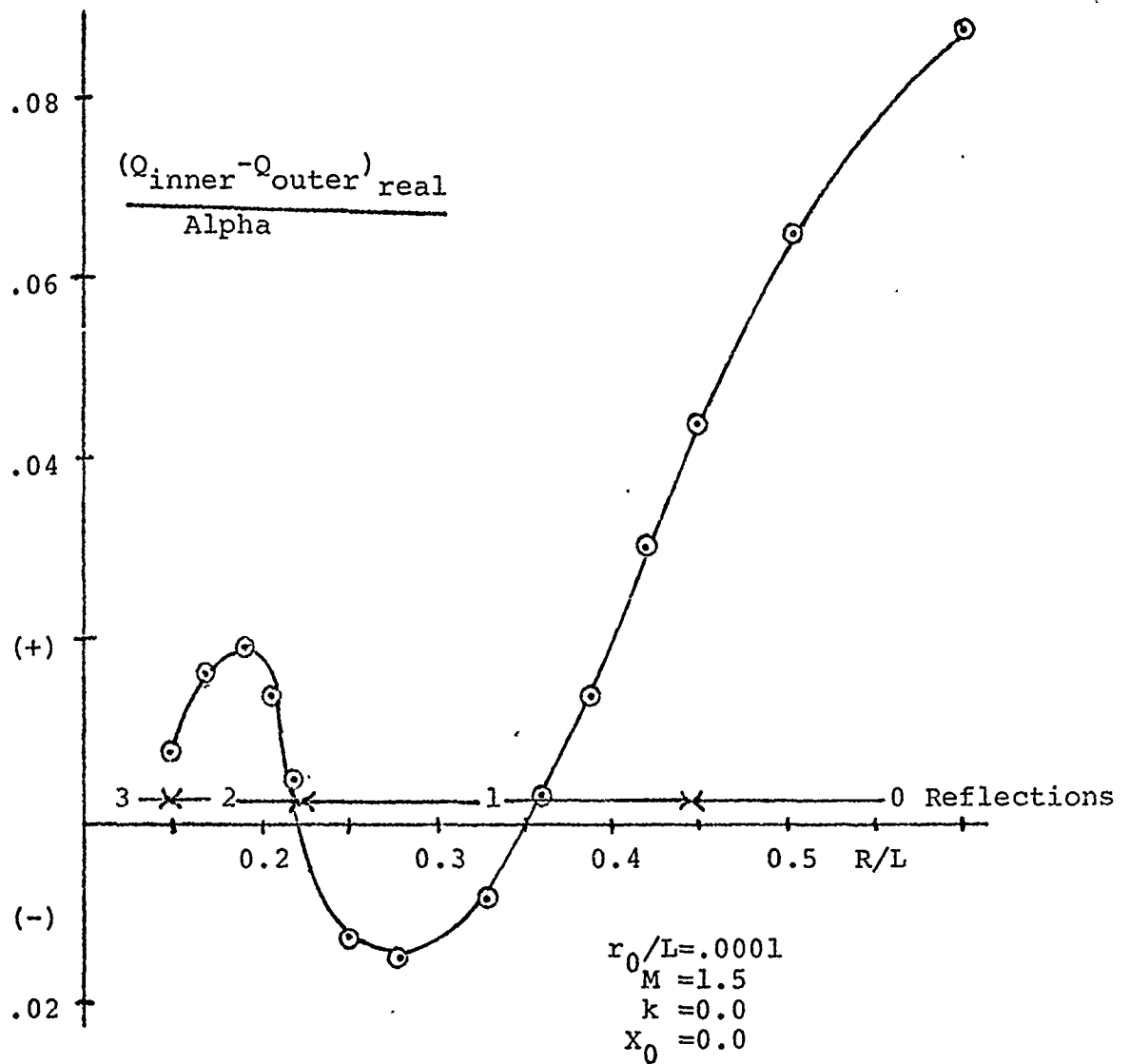


Figure 22 - PITCHING MOMENT VS OUTER RADIUS-TO-LENGTH RATIO

$R/L = .3$
 $r_0/L = .0001$
 $M = 1.5$
 $k = 0.0$

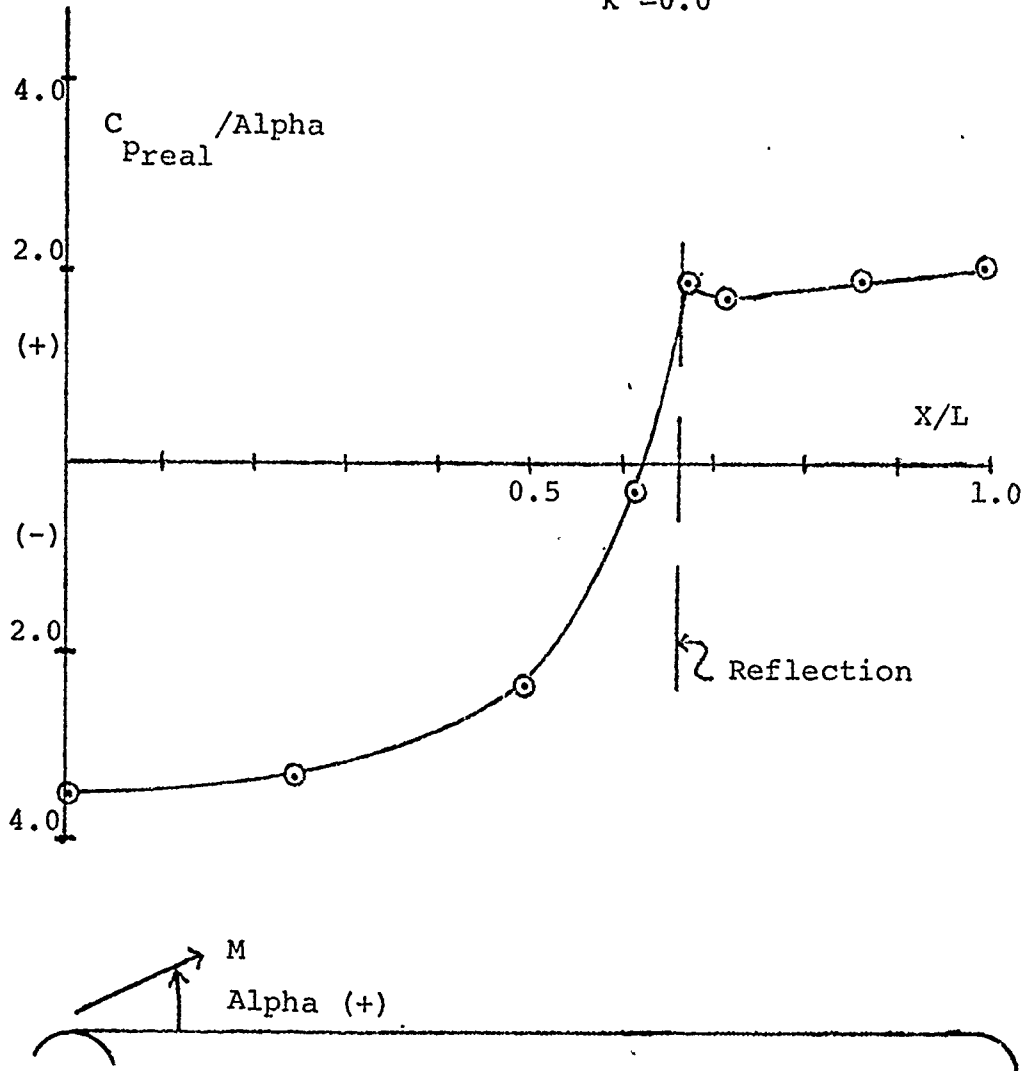


Figure 23 - REPRESENTATIVE AXIAL PRESSURE DISTRIBUTION INCLUDING ONE REFLECTION

XIII. CONCLUSIONS AND RECOMMENDATIONS

The computer programs of references 12 and 13 have been successfully adapted to the case of a ring wing in supersonic flow undergoing oscillations in angle of attack. Available cases for comparison have shown good agreement, indicating the validity of the method. The programs make possible the relatively easy calculation of the unsteady lifts and moments of a ring wing in supersonic flow, for such applications as tubular artillery shells (STUP, spinning tubular projectile), although spin may induce aerodynamic effects not accounted for in the method. Further evaluation and parametric studies are recommended for a more complete verification of the computer programs.

APPENDIX A

ISENTROPIC THRUST CALCULATIONS

Isentropic thrust calculations made use of standard isentropic relations. Calculations were based on plenum pressure and nozzle exit area. The formula for isentropic thrust is arrived at as follows. Nozzle thrust may be written in the following form:

$$T_s = w V_{ex} = (\rho A M^2 \gamma R T)_{ex}$$

where w is nozzle mass flow, A is exit area, and one has applied the speed of sound relation. Exit Mach number may be written in terms of pressure ratio as follows:

$$M_{ex} = \frac{2}{\gamma-1} \left(\left(\frac{P_0}{P_{ex}} \right)^{\gamma-1/\gamma} - 1 \right)$$

Applying this and the state equation to the formula for T_s one obtains:

$$T_s = P_{ex} A_{ex} \frac{2}{\gamma-1} \left(\left(\frac{P_0}{P_{ex}} \right)^{\gamma-1/\gamma} - 1 \right)$$

Now, once one has measured plenum and ambient pressure, and thrust, T_{exp} , one can calculate the isentropic thrust efficiency:

$$\eta = T_{exp} / T_s$$

APPENDIX B

ENTRAINMENT RATIO CALCULATIONS

Mass flows and entrainment ratios were calculated according to the equations and procedures set out in reference 11, the ASME Power Test Codes. The equation for mass flow, from reference 11 is:

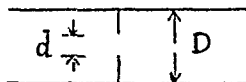
$$w = 359 c f d^2 Fa Y \sqrt{hp} \quad , \text{lb/hr}$$

where:

c Discharge Coefficient

$$f = 1/\sqrt{1-\beta^4} \quad \beta = d/D$$

d and D



Fa Thermal Expansion Factor

Y (Ya for a venturi) Adiabatic Expansion Factor

h The pressure drop across the device, in inches of water

ρ Density of the fluid being metered, pounds per cubic foot

If w1 is the entrained flow and w2 the primary, then (w1 uses a venturi, w2 an orifice):

$$\frac{w_1}{w_2} = \frac{c_1}{c_2} \frac{f_1}{f_2} \left(\frac{d_1}{d_2}\right)^2 \frac{Fa_1}{Fa_2} \frac{Ya_1}{Y_2} \sqrt{\frac{h_1}{h_2}}$$

Non-geometric factors for the primary flow, such as discharge coefficient, could be reasonably approximated for all tests as:

$$C2=.65 \quad Fa2=1.0 \quad Y2=.99$$

In the case of the entrained flow these factors had to be changed for each test axial location, due to the widely varying flow requirements. The geometric factors above had the following fixed values:

$$F1=1.0328 \quad d1=.75 \quad F2=1.0792 \quad d2=1.11$$

Now, entrainment ratio is commonly written as:

$$\frac{M}{M_0} = \frac{w_1 + w_2}{w_2} = \frac{w_1}{w_2} + 1$$

Using the previous formula for w_1/w_2 , the entrainment ratio may now be written as:

$$\frac{M}{M_0} = A \frac{\sqrt{h_1}}{h_2} + 1$$

where A is the combination of the ratios of factors previously listed. This equation was used to calculate the nozzle entrainment ratios.

APPENDIX C

ENTRAINMENT CHAMBER DESIGN

The entrainment chamber design was closely based on previous work by Ricou and Spalding (reference 7), and Peschke (reference 8). Peschke's report especially was a good source of specific design data, while Ricou and Spalding was primarily a source of the design principles.

The entrainment chamber consisted essentially of a central porous cylinder, closed at one end with a solid wall through which the nozzle protruded, the other end being open to the outside. Orifice plates of specific diameters were constructed and mated to cylinders of specific length, length and diameter specified according to the data available in Peschke. These orifice cylinders were of such outside diameter that they fit closely inside the porous cylinder, into which they were inserted for the measurement of mass flow at the various jet axial positions corresponding to the orifice diameters. The purpose of the orifice was to seal the open end such that entrained air could only enter through the porous cylinder. The purpose of the orifice cylinder was to seal off that portion of the porous cylinder beyond the jet axial position where flow was being measured. The porous cylinder was surrounded everywhere, except at the open end, by a box, also encasing the nozzle plenum, which served as the membrane air supply.

The entrainment chamber was about 4 by 4 feet square and 4 feet high, supported on 3 foot legs. The porous cylinder

was 30 inches in diameter and 25 inches long. Orifice diameters used, corresponding to the listed jet axial positions, were as follows:

Diameter	X/D
1.75	2.5
3.0	5.0
6.5	13.0

The entrainment chamber box, legs, orifice plates and porous cylinder frame work were all constructed of wood. The orifice cylinders were made of fiberglass sheet and the porous covering to the porous cylinder frame work was two layers of dacron crepe cloth, as suggested in Peschke's report.

One critical chamber design parameter was orifice diameter. It is clear that too small an orifice would interfere with the jet being measured, while too large an orifice would not properly restrict the entrained flow to entering only through the membrane, thus preventing the creation of a readable pressure gradient across the orifice. The approach to this problem in both references 7 and 8 was to find an optimal orifice size at a specific jet axial location by testing several orifice sizes. To minimize orifice construction, this investigation took a different approach. That was to use the reference 8 orifice data as a starting point, and vary the orifice axial location, such that a readable pressure gradient was created while not interfering with the jet. In both approaches the attempt is to optimize the orifice diameter, jet axial location combination.

One primary difference between this chamber's geometry and that of others (references 7 and 8) should be noted. As shown in figure 8, exit orifices were positioned in the porous cylinder at various distances from the nozzle. That portion of the porous cylinder extending above the orifice plate was sealed by a fiberglass cylinder attached to the orifice. Thus in this situation, that portion of the jet beyond the orifice, and inside the porous cylinder exit, was not in a truly free jet flow situation. This was as opposed to the reference 7 and 8 configurations where the exit orifice corresponded to the exit of the porous cylinder. Thus in those experiments the jet past the orifice was in a truly free jet flow situation. The configuration used in this report was adopted in order to facilitate the measurement of mass flows at many axial locations. It was hoped that this chamber's geometry would not affect the chamber readings greatly, although some effect was to be expected.

An important problem, again with regard to the chamber orifices, concerned the measurement of the pressure differential across the orifice. Both reference 7 and 8 indicated that a measurement accuracy of .001 inches of water was required. Reference 7 used a micro manometer while reference 8 used a pressure transducer for this purpose. After the entrainment chamber was constructed experience showed that such accuracies were required. This investigation used an alcohol micro manometer which provided an accuracy of .0001 inches of manometric fluid. This accuracy was obtained through the combination of an inclined tube, hairline indicator, magnifying lens and a micrometer adjustment to indicator level.

Flow measurement devices for the primary and entrained flow were an orifice and venturi respectively. These were constructed and used according to ASME Power Test Codes

specifications (reference 11). Based on these specifications, an inclined water manometer was found to be necessary for measuring the orifice pressure drop, while a vertical mercury manometer was sufficient for the venturi.

APPENDIX D

PROGRAM LISTINGS AND DOCUMENTATION

This appendix contains basic program and input descriptions for the two programs used, from references 12 and 13. The programs also are listed in their modified form for the computation of a ring wing at angle of attack. The program statements relevant to the modification are indicated in the program listings. Also indicated in the interior flowfield program is the statement whose omission caused the numerical instability noted in reference 12.

The inner flow field program consists of 8 subroutines, and a main program which manipulates each of these. The action of each particular subroutine is indicated in the program listing. Inputs are made by way of a Fortran Namelist. The input parameters are, in proper order:

- FSTRMN Free stream mach number.
- REDFRQ The reduced frequency.
- RO The outer cylinder radius to length ratio.
- RI The inner cylinder radius to length ratio.
- NGRDFN Grid fineness, or the number of grid points taken on the first right running mach line.
- N Circumferential mode number.
- M Axial mode number.
- M1 The m in Q_{mn} , the generalized aerodynamic force.

IPRINT An output parameter. 0 indicates only basic output. 1 indicates output including such things as Phi and its derivatives at each flow field point.

Of the above inputs, in the modified program, the inputs N, M, and M1 must be set to 1, as the case under consideration is not panel flutter but a cylinder at angle of attack. The other inputs are arbitrary.


```

IF ( (X(1)+EPS) .GE. 1. ) GO TO 8
IHAVEP = IHAVEP + 1
GO TO 1
C
6 CALL RAD1
IHAVEP = 0
LCOUNT = LCOUNT + 1
GO TO 1
C
8 CONTINUE
IF ( ABS(XPT(LCOUNT) - 1. ) .LE. EPS ) GO TO 10
L = LCOUNT
LM1 = LCOUNT - 1
LM2 = LCOUNT - 2
XPT(L) = 1.
CPR(L) = ENDPT(CPR(LM1),CPR(LM2),1.00,XPT(LM1),DSTSTR)
CPI(L) = ENDPT(CPI(LM1),CPI(LM2),1.00,XPT(LM1),DSTSTR)
C
C
WRITE(6,105)
DO 9 I = 1,L
ARG = RM1*PI*XPT(I)
C
C
THE FOLLOWING TWO CARDS WERE MODIFIED FROM THE ORIGINAL REFERENCE 12 PROGRAM.
C
C
DUMMY(I)=CPR(I)*.1*XPT(I)
9 DUNCE(I)=CPI(I)*.1*XPT(I)
C
SUM1 = 0.5*(CPR(L) + CPR(LM1))*(1.00 - XPT(LM1))
SUM2 = 0.5*(CPI(L) + CPI(LM1))*(1.00 - XPT(LM1))
C
WRITE(6,114) FSTRMN,REDFRQ,RO,RI,N
C
CALL QSF(DSTSTR,DUMMY,DUMMY,LM1)
CALL QSF(DSTSTR,DUNCE,DUNCE,LM1)
QREAL = 0.5*(DUMMY(LM1) + SUM1)
QIMAG = 0.5*(DUNCE(LM1) + SUM2)
C
WRITE(6,115) M,M1,QREAL,M,M1,QIMAG
GO TO 12
C
10 CONTINUE
XPT(L) = 1.
WRITE(6,105)
DO 11 I = 1,LCOUNT
ARG = RM1*PI*XPT(I)
DUMMY(I)=CPR(I)*.1*XPT(I)
11 DUNCE(I)=CPI(I)*.1*XPT(I)
C
WRITE(6,114) FSTRMN,REDFRQ,RO,RI,N
C
CALL QSF(DSTSTR,DUMMY,DUMMY,L)
CALL QSF(DSTSTR,DUNCE,DUNCE,L)
QREAL = 0.5*DUMMY(L)
QIMAG = 0.5*DUNCE(L)
WRITE(6,115) M,M1,QREAL,M,M1,QIMAG
C
12 CONTINUE
WRITE(6,998)
998 FORMAT('1', 'CP REAL')
CALL PLOT(XPT,CPR,LCOUNT,0)
WRITE(6,999)
999 FORMAT('1', 'CP IMAGINARY')
CALL PLOT(XPT,CPI,LCOUNT,0)
STOP
150 FORMAT(F10.5)
105 FORMAT('1',T19,'I',T27,'X',T38,'CPR',T50,'CPI',//)
110 FORMAT('0',15X,I5,3(3X,F9.5))
114 FORMAT('/',T20,'MACH NUMBER = ',F10.7,/' ',T20,
1 'REDUCED FREQUENCY = ',F10.7,/' ',T20,'(RADIUS/
2 'LENGTH) OUTER = ',F10.7,/' ',T20,'(RADIUS/LENGTH)'

```



```

C      COMPLEX PHI(400),DPHIS1(400),DPHIS2(400)
      DIMENSION X(400),R(400),XPT(400),CPR(400),CPI(400)
      COMMON/BLCK1/ FSTRMN,DELTAS,DX,DH,DSTSTR,RO,RI,REDFRQ
      COMMON/BLCK2/ A1,A2,A3,A4,RN,RM,RM1,FACT1,FACT2
      COMMON/BLCK3/ NGRDFN,NPTS,LCOUNT,IHAVEP,N,M,M1,IPRINT
      COMMON/BLCK4/ PHI,DPHIS1,DPHIS2
      COMMON/BLCK5/ X,R,XPT,CPR,CPI
      DATA PI/3.141593/

C      X(1) = 0.
      R(1) = RO
      XPT(1) = 0.

C      C
C      C      ALONG THE INITIAL RIGHT RUNNING CHARACTERISTIC PHI AND
C      C      DPHIS2 ARE ZERO.
C      C
C      PHI(1) = (0.,0.)
      DPHIS2(1) = (0.,0.)

C      C
      AA=.2/FSTRMN
      DPHIS1(1) = CMPLX(AA,0.)
      DPHIDR = A4*DPHIS1(1)
      DPHIDX = A2*DPHIS1(1)
      CPR(1) = -2.*REAL(DPHIDX)
      CPI(1) = -2.*AIMAG(DPHIDX)

C      C
      IF ( IPRINT .NE. 1 ) RETURN
      WRITE(6,90)
      WRITE(6,95)
      WRITE(6,100) X(1),DPHIS1(1),DPHIS2(1),PHI(1),
1      R(1),DPHIDR,DPHIDX
      WRITE(6,110) CPR(1),CPI(1)
      RETURN
90  FORMAT('1',T10,'X',T22,'D(PHI)/D(S1)',T46,
1      'D(PHI)/D(S2)',T70,'PHI')
95  FORMAT('1',T10,'R',T23,'D(PHI)/DR',T47,'D(PHI)/DX',/)
100 FORMAT(3H 1,2X,F8.4,4X,3(F12.5,F9.5,3X),/' ',4X,F8.4,
1      4X,3(F12.5,F9.5,3X))
110 FORMAT('0',10X,'INITIAL VALUE: INNER SURFACE OF',
1      ' OUTER CYLINDER',/' ',30X,'CP(REAL) = ',F8.4,10X,
2      'CP(IMAG) = ',F8.4,/)
      END

C      C      THIS IS SUBROUTINE COMPRX
C      C
      SUBROUTINE COMPRX
C      C
      SUBROUTINE COMPRX COMPUTES THE (X,R) COORDINATES OF A
      C      C      GRID POINT.
      C      C
      DIMENSION X(400),R(400),XPT(400),CPR(400),CPI(400)
      COMMON/BLCK1/ FSTRMN,DELTAS,DX,DH,DSTSTR,RO,RI,REDFRQ
      COMMON/BLCK3/ NGRDFN,NPTS,LCOUNT,IHAVEP,N,M,M1,IPRINT
      COMMON/BLCK5/ X,R,XPT,CPR,CPI

C      C
      I = IHAVEP + 1
      J = IHAVEP

C      C
      IF THIS IS THE FIRST POINT ON A NEW RIGHT RUNNING MACH
      C      C      LINE, GO TO 1.
      C      C
      IF ( J .EQ. 0 ) GO TO 1

C      C
      X(I) = X(J) + DX
      R(I) = R(J) - DH
      RETURN

C      C
1      R(I) = RO
      X(I) = X(1) + DSTSTR
      RETURN
      END

C      C      THIS IS SUBROUTINE MACHLN

```


C
C
C
C
C

THE FOLLOWING VARIABLE, IK, WAS FOUND TO BE UNDEFINED IN THE ORIGINAL REFERENCE 12 PROGRAM, AND WAS THE REASON FOR A NUMERICAL INSTABILITY AFTER THE FIRST REFLECTION.

C
C
C
C
C

```

IK=CMPLX(0.0,REDFRQ)
AA1 = 1. - A1/R(I)
A = CMPLX(AA1,A3)
B1 = A1/R(I) - 0.25*DELTAS*DELTAS*(FACT1 -
1 FACT2/(R(I)*R(I)))
B = CMPLX(B1,A3)
C1 = 1. + A1/R(J)
C2 = -A1/R(J) + 0.25*DELTAS*DELTAS*(FACT1 -
1 FACT2/(R(I)*R(I)))
C3 = (2.*FACT1 - FACT2/(R(J)*R(J)) -
1 FACT2/(R(I)*R(I)))*DELTAS*0.5
C = DPHIS1(J)*CMPLX(C1,-A3) + DPHIS2(J)*CMPLX(C2,-A3)
1 + PHI(J)*CMPLX(C3,0.)

```

C
C
C
C
C
C

```
IF ( MOD(N,2) .EQ. 0 ) GO TO 1
```

APPLY THE BOUNDARY CONDITION FOR ODD VALUES OF N. CP = (IK)PHI + DPHIDX = 0. USE THIS B.C., THE FINITE DIFFERENCE EQN. FOR DPHIDX, AND THE EQN. FOR THE RIGHT RUNNING MACHLINE TO SOLVE FOR DPHIS1 AND DPHIS2.

```

DELTA = A2 + 0.5*IK*DELTAS
GAMMA = IK*( PHI(J) + 0.5*DELTAS*DPHIS2(J) )

```

C
C
C

SOLVING FOR DPHIS1 AND DPHIS2

```

DPHIS1(I) = ( C + B*GAMMA/DELTA )/( A - B*A2/DELTA )
DPHIS2(I) = ( C - A*DPHIS1(I) )/B

```

C

```

DPHIDX = A2*( DPHIS1(I) + DPHIS2(I) )
DPHIDR = A4*( DPHIS1(I) - DPHIS2(I) )
GC TO 2

```

C
C
C

APPLY THE BOUNDARY CONDITION FOR EVEN VALUES OF N.

```

1 DPHIS1(I) = C/(A+B)
DPHIS2(I) = DPHIS1(I)
DPHIDR = (0.,0.)
DPHIDX = A2*(DPHIS1(I) + DPHIS2(I))

```

C
C
C
C

PHI.

```
2 PHI(I) = PHI(J) + 0.5*(DPHIS2(J) + DPHIS2(I))*DELTAS
```

```

IF ( IPRINT .NE. 1 ) RETURN
WRITE(6,100) X(I),DPHIS1(I),DPHIS2(I),PHI(I),
1 R(I),DPHIDR,DPHIDX
RETURN

```

```

100 FORMAT(3H RI,2X,F8.4,4X,3(F12.5,F9.5,3X),/' ',4X,F8.4,
1 4X,3(F12.5,F9.5,3X))

```

C
C
C
C
C
C

END THIS IS SUBROUTINE RAD2

SUBROUTINE RAD2

SUBROUTINE RAD2 COMPUTES THE FLOW FIELD QUANTITIES AT THE INNER SURFACE OF THE OUTER CYLINDER, WHERE THE FLOW TANGENCY CONDITION PRESCRIBES DPHIDR.

```

CCOMPLEX D,E,F,TANR
CCOMPLEX DPHIDR,DPHIDX
CCOMPLEX PHI(400),DPHIS1(400),DPHIS2(400)
DIMENSION X(400),R(400),XPT(400),CPR(400),CPI(400)
CCOMMON/BLCK1/ FSTRMN,DELTAS,DX,DH,DSTSTR,RO,RI,REDFRQ
CCOMMON/BLCK2/ A1,A2,A3,A4,RN,RM,RM1,FACT1,FACT2
CCOMMON/BLCK3/ NGRDFN,NPTS,LCOUNT,IHAVEP,N,M,M1,IPRINT

```

```

COMMON/BLCK4/ PHI,DPHIS1,DPHIS2
COMMON/BLCK5/ X,R,XPT,CPR,CPI
DATA PI/3.141593/

C
I = IHAVEP + 1
J = IHAVEP + 2
K = LCOUNT
ARG=RM*PI*X(I)

CCCC
CALCULATE THE COEFFICIENTS ASSOCIATED WITH THE LEFT
RUNNING MACH LINE.

D1 = A1/R(I) + 0.25*DELTAS*DELTAS*(FACT1 - FACT2/(R(I)
1 *R(I)))
D = CMPLX(D1,-A3)
E1 = -1. - A1/R(I)
E = CMPLX(E1,-A3)
F1 = -A1/R(J) - 0.25*DELTAS*DELTAS*(FACT1 - FACT2/
1 (R(I)*R(I)))
F2 = -1. + A1/R(J)
F3 = (2.*FACT1 - FACT2/(R(I)*R(I)) - FACT2/(R(J)*
1 R(J)))*DELTAS*0.5
F = DPHIS1(J)*CMPLX(F1,A3) + DPHIS2(J)*CMPLX(F2,A3) -
1 PHI(J)*CMPLX(F3,0.)

CCCC
CALCULATE THE FLOW TANGENCY CONDITION - TANR
BOUNDARY CONDITIONS FOR PANEL FLUTTER

CCCC
THE FOLLOWING THREE CARDS WERE MODIFIED FROM THE ORIGINAL
REFERENCE 12 PROGRAM.
C

ALPHA=.1
TANR1=ALPHA
TANR2=REDFRQ*X(I)*ALPHA
TANR = CMPLX(TANR1,TANR2)

C
DPHIS1(I) = ( F + TANR*E/44 )/( D + E )
DPHIS2(I) = ( F - TANR*D/44 )/( D + E )
DPHIDR = A4*(DPHIS1(I) - DPHIS2(I))
DPHIDX = A2*(DPHIS1(I) + DPHIS2(I))

C
INTEGRATE ALONG THE LEFT RUNNING MACH LINE TO FIND PHI
PHI(I) = PHI(J) + 0.5*(DPHIS1(J) + DPHIS1(I))*DELTAS
C
CALCULATE THE PRESSURE COEFFICIENT AT THIS GRID POINT.
C
XFT(K) = X(I)
CPR(K) = -2.*(-REDFRQ*AIMAG(PHI(I)) + REAL(DPHIDX))
CPI(K) = -2.*(REDFRQ*REAL(PHI(I)) + AIMAG(DPHIDX))

C
IF ( IPRINT .NE. 1 ) RETURN
WRITE(6,100) X(I),DPHIS1(I),DPHIS2(I),PHI(I),
1 R(I),DPHIDR,DPHIDX,TANR
WRITE(6,110) CPR(K),CPI(K)
RETURN
100 FORMAT(3H RO,2X,F8.4,4X,3(F12.5,F9.5,3X),/' ',4X,F8.4,
1 4X,3(F12.5,F9.5,3X))
110 FORMAT('0',10X,'INNER SURFACE OF OUTER CYLINDER',/' ',
1 30X,'CP(REAL) = ',F8.4,10X,'CP(IMAG) = ',F8.4,/'//)
END

C
THIS IS SUBROUTINE GENFPT

C
SUBROUTINE GENFPT( IER )

C
SUBROUTINE GENFPT COMPUTES THE FLOW FIELD QUANTITIES
AT A GENERAL FLOW FIELD POINT.

C
COMPLEX PHI

```



```

1   Y(4))
   SUM1=Y(2)+Y(2)
   SUM1=SUM1+SUM1
   SUM1=HT*(Y(1)+SUM1+Y(3))
   Z(1)=0.
   AUX1=Y(3)+Y(3)
   AUX1=AUX1+AUX1
   Z(2)=SUM2-HT*(Y(2)+AUX1+Y(4))
   IF(NDIM-5)10,9,9
9   AUX1=Y(4)+Y(4)
   AUX1=AUX1+AUX1
   Z(5)=SUM1+HT*(Y(3)+AUX1+Y(5))
10  Z(3)=SUM1
   Z(4)=SUM2
   RETURN
C
C   NDIM IS EQUAL TO 3
11  SUM1=HT*(1.25*Y(1)+Y(2)+Y(2)-.25*Y(3))
   SUM2=Y(2)+Y(2)
   SUM2=SUM2+SUM2
   Z(3)=HT*(Y(1)+SUM2+Y(3))
   Z(1)=0.
   Z(2)=SUM1
12  RETURN
   END

```

The outer flowfield program, from reference 13, consists of 5 subroutines and a main program to manipulate the subroutines. The action of each particular subroutine is indicated in the program listing. Inputs required to the program must be on two cards, and are as follows:

DATE

MACH Mach number.

RADIUS Radius to length ratio.

K Reduced frequency.

MFREQ Axial mode number.

NR The r in Q_{mr} , the generalized aerodynamic force.

NFREQ Circumferential mode number.

FINGRD Grid fineness, essentially the number of grid points along the cylinder surface.

The run date is typed onto the first card. The second card contains the above parameters in the following format: F20.8, 2F10.3, 4I5. Of the above parameters, in the modified program, MFRFQ, NR, and NFREQ must be set to 1, as the case under consideration is not panel flutter but a cylinder at angle of attack. Other parameters are arbitrary.

```

00000010
00000020
00000030
00000040
00000050
00000060
00000070
00000080
00000090
00000100
00000110
00000120
00000130
00000140
00000150
00000160
00000170
00000180
00000190
00000200
00000210
00000220
00000230
00000240
00000250
00000260
00000270
00000280
00000290
00000300
00000310
00000320
00000330
00000340
00000350
00000360
00000370
00000380
00000390
00000400
00000410
00000420
00000430
00000440
00000450
00000460
00000470

C C C C LINEARIZED METHOD OF CHARACTERISTICS
FOR SUPERSONIC FLOW PAST A VIBRATING CYLINDRICAL SHELL

DIMENSION DATE(3)
DIMENSION XN(400)
COMMON DPHI1,DPHIK,PHI(400,2),PHK(400,2),IPHI1,IPHI2,
4 IKM,IKW,PARM,W,II,REALCP(400),CP(400),AMAGCP(400),
1 X(400,2),R(400,2),NREQ,FINGRD,ISWITCH,JSWITCH,ILINE,MLINE,JLINE,
2 MFREQ,IHAVEP,KOUNT
3 INTEGER I,HAVEP,FINGRD
REAL MACH,MANGL,K
CCOMPLEX DPHI1,DPHIK,PHI,IKM,CP,PX,IPHI1,IPHI2,IKW,PHK,II,QPHI,PR

PRINT NAME OF PROGRAM AND DATE OF RUN

READ (5,10)DATE
FORMAT (3A4)
FORMAT (11,///,40X,'LINEARIZED METHOD OF CHARACTERISTICS',//40X,
1 'FOR SUPERSONIC FLOW PAST A VIBRATING CYLINDRICAL SHELL',//20X
2 'DATE OF RUN-',3A4///)
WRITE (6,11) DATE

READ INPUT
READ(5,1)MACH,RADIUS,K,MFREQ,NR,NREQ,FINGRD
1 FORMAT(F20.8,2F10.3,4I5)

COMPUTE CONSTANTS
II=(0.0,1.0)
BETA=SQRT(MACH**2-1.0)
MANGL=AR SIN(1.0/MACH)
XLENGT=1/(2.*COS(MANGL))
HEIGHT=SIN(MANGL)*XLENGT
DELTA=XLENGT/FINGRD
DSTSTR=DELTA*S*COS(MANGL)*2.0
HDSTR=5*DSTSTR
ML=IFIX(FINGRD+1.0)
TRNGLH=HDSTR*TAN(MANGL)

SET COUNTERS
ISWITCH=2
JSWITCH=1
IHAVEP=1
KOUNT=1

```



```

00000880
00000890
00000900
00000910
00000920
00000930
00000940
00000950
00000960
00000970
00000980
00000990
00001000
00001010
00001020
00001030
00001040
00001050
00001060
00001070
00001080
00001090
00001100
00001110
00001120
00001130
00001140
00001150
00001160
00001170
00001180
00001190
00001200
00001210
00001220
00001230
00001240
00001250
00001260
00001270

```

```

C      TEST WHE. HER THIS IS A SURFACE POINT.
C      IF (IHAVEP.EQ.KOUNT) GO TO 40
C      GO TO 60
C 30    CALL MACHLN
C      GO TO 50
C 40    CALL PANPNT
C      GO TO 50
C 60    CALL GENFPT
C      A=IHAVEP
C      B=ISWITCH/(2.0*BETA))*(PHK(A,B)+ PHI(A,B))
C      PX=((MACH/2.0)*(PHK(A,B)-PHI(A,B)))
C      IF (IHAVEP.EQ.KOUNT) GO TO 25
C      GO TO 35
C      INCREMENT FOR NEXT LINES
C 25    IF (ISWITCH.EQ.1.) GO TO 103
C      ISWITCH=1
C      JSWITCH=2
C      IHAVEP=1
C      GO TO 108
C 103   ISWITCH=2
C      JSWITCH=1
C      IHAVEP=1
C      GO TO 108
C      AT 35 INCREMENT ALONG PRESENT LINE
C 35    IHAVEP=IHAVEP+1
C      GO TO 104
C 108   KOUNT=KOUNT+1
C      IF ((KOUNT-1).EQ.ML)GO TO 101
C      GO TO 104
C 101   CONTINUE
C      CALL INTEG(REALCP,MFREQ,NR,DSTSTR,ML)
C      CALL INTEG(AMAGCP,MFREQ,NR,DSTSTR,ML)
C      THE FOLLOWING CARDS WERE MODIFIED FROM THE ORIGINAL.
C      REFERENCE 13 PROGRAM TO ENABLE GRAPHICAL CP OUTPUT.
C      XN(I)=0.0
C      DO 115 I=1,ML
C      XN(I+1)=XN(I)+1./ML

```

```

C
C
C

```

```

115 CONTINUE
198 WRITE(6,999)
    WFORMAT(1,1,CP,REAL,')
    CALL PLOTP(XN,REALCP,ML,0)
    WRITE(6,999)
    WFORMAT(1,1,CP,IMAGINARY,')
    CALL PLOTP(XN,AMAGCP,ML,0)
    STOP
    END
C SUBROUTINE COMPR
C REAL MACH,MANGL,K,KW
C COMPUTES THE X AND R COORDINATES
COMMON DPHII,DPHIK,PHI(400,2),PHK(400,2),QPHI(400,2),IPHI1,IPHI2,
1 IKM,IKW,PARW,W,II,REALCP(400),CP(400),AMAGCP(400),
2 MACH,K,MANGL,RADIUS,DELTA,SL,XTAS,XLENGT,BETA,DSTSTR,HDSTRL,TRNGLH,
3 X(400,2),R(400,2),NFREQ,FINGRD,ISWTC,JSWTC,I,LINE,MLINE,JLINE,
4 MFREQ, IHAVEP,KOUNT
C COMPLEX DPHII,DPHIK,PHI,IKM,CP,PX,IPHI1,IPHI2,IKW,PHK,II,QPHI,PR
C INTEGER FINGRD
TEST FOR POINT ON MACH LINE
IF (IHAVEP.EQ.1) GO TO 10
I=IHAVEP-1
J=1-I
X(I,ISWTC)=X(J
R(I,ISWTC)=R(J
RETURN
I=IHAVEP
X(I,ISWTC)=X(I
R(I,ISWTC)=R(I
RETURN
END ROUTINE MACHLN
COMMON DPHII,DPHIK,PHI(400,2),PHK(400,2),QPHI(400,2),IPHI1,IPHI2,
1 IKM,IKW,PARW,W,II,REALCP(400),CP(400),AMAGCP(400),
2 MACH,K,MANGL,RADIUS,DELTA,SL,XTAS,XLENGT,BETA,DSTSTR,HDSTRL,TRNGLH,
3 X(400,2),R(400,2),NFREQ,FINGRD,ISWTC,JSWTC,I,LINE,MLINE,JLINE,
4 MFREQ, IHAVEP,KOUNT
C REAL MACH,MANGL,K,KW
C COMPLEX
1 A,B,C,D,DPHI1,DPHIK,PHI,IKM,CP,PX,IPHI1,IPHI2,IKW,PHK,II,QPHI
2 ,PR
C INTEGER FINGRD

```

```

00001280
00001290
00001300
00001310
00001320
00001330
00001340
00001350
00001360
00001370
00001380
00001390
00001400
00001410
00001420
00001430
00001440
00001450
00001460
00001470
00001480
00001490
00001500
00001510
00001520
00001530
00001540
00001550
00001560
00001570
00001580
00001590
00001600
00001610
00001620
00001630
00001640
00001650
00001660
00001670
00001680

```

```

I=IHAVEP
PHK(I,ISWITCH)=(0.,0.)
A=1.+DELTA/(4.*R(I,ISWITCH)*MACH)+0.5*IKM*DELTA
AA2=1.-DELTA/(4.*R(I,JSWITCH)*MACH)-0.5*IKM*DELTA
PHI(I,ISWITCH)=PHI(I,JSWITCH)*{AA2/A}
QPHI(I,ISWITCH)=(0.,0.)
RETURN
END
SUBROUTINE GENFPT
GENFPT COMPUTES THE VELOCITY POTENTIAL AND ITS DERIVATIVES AT A
GENERAL FLOW FIELD POINT.
COMMON DPHI1,DPHIK,PHI(400,2),PHK(400,2),IPHI1,IPHI2,
4 IKM,IKW,PARW,W,II,REALCP(400),CA(400),AMAGCP(400),
1 MACH,K,MANGL,RADIUS,DELTA,XLENGT,BETA,DSTSTR,HDSTRL,TRNGLH,
2 X(400,2),R(400,2),NFREQ,FINGRD,ISWITCH,ILINE,MLINE,JLINE,
3 MFREQ,IHAVEP,KOUNT
REAL MACH,MANGL,K,KW,N
COMPLEX AA1,AA2,AA3
1 A,B,C,D,DPHI1,DPHIK,PHI,IKM,CP,PX,IPHI1,IPHI2,IKW,PHK,II,QPHI
2 ,PR,EF
3 INTEGER FINGRD
I=IHAVEP
J=IHAVEP -1
N=FLOAT(NFREQ)
A=1.-DELTA/(4.*R(I,ISWITCH)*MACH)+0.5*IKM*DELTA
AA1=1.+DELTA/(4.*R(J,ISWITCH)*MACH)-0.5*IKM*DELTA
AA3=-1.+DELTA/(4.*R(I,JSWITCH)*MACH)+0.5*IKM*DELTA
B=DELTA/(4.*R(I,ISWITCH)*MACH)+0.5*IKM*DELTA-0.25*DELTA**2*
1 {K**2-(N**2/(R(I,ISWITCH)**2*MACH**2))}
C=PHK(J,ISWITCH)*AA1+PHI(J,ISWITCH)*(-DELTA/(4.*R(J,ISWITCH)*MACH)
1 -0.5*IKM*DELTA+0.25*DELTA**2*(K**2-(N**2/(R(I,ISWITCH)**2*MACH**
2 2)))+QPHI(J,ISWITCH)*DELTA*0.5*(K**2-N**2/(R(J,ISWITCH)**2*MACH
3 **2))+QPHI(J,ISWITCH)*DELTA*0.5*(K**2-N**2/(R(I,ISWITCH)**2*
4 MACH**2))
D=DELTA/(4.0 *R(I,ISWITCH)*MACH)-0.5 *IKM*DELTA+0.25 *DELTA**2
12*(K**2-(N**2/(R(I,ISWITCH)**2*MACH**2)))

```

```

00001690
00001700
00001710
00001720
00001730
00001740
00001750
00001760
00001770
00001780
00001790
00001800
00001810
00001820
00001830
00001840
00001850
00001860
00001870
00001880
00001890
00001900
00001910
00001920
00001930
00001940
00001950
00001960
00001970
00001980
00001990
00002000
00002010
00002020
00002030
00002040
00002050
00002060
00002070
00002080
00002090
00002100
00002110
00002120
00002130
00002140
00002150
00002160

```

10


```

3**2))+ QPHI(J, ISWTC H)*DELTAS*0.5*(K**2~ N**2/(R(I, ISWTC H)**2*
4 MACH**2))
C
PHK(I, ISWTC H)= (C+B*(2.0/MACH)*(PARW+IKW))/(A+B)
PHI(I, ISWTC H)= (-A*(2.0/MACH)*(PARW+IKW)+C)/(A+B)
C
QPHI(I, ISWTC H), ISWTC H)=QPHI(J, ISWTC H)+0.5*(PHI(J, ISWTC H)+PHI(I
, ISWTC H))*DELTAS
1 PX=(MACH/(2.0*BETA))*((PHK(I, ISWTC H)+PHI(I, ISWTC H))
CP(KOUNT)=-2.0*(I*K*QPHI(I, ISWTC H)+PX)
REALCP(KOUNT)=REAL(CP(KOUNT))
AMAGCP(KOUNT)=AIMAG(CP(KOUNT))
RETURN
END
SUBROUTINE INTEG(Y, M, NR, DX, ML)
DIMENSION Y(ML)
Q=0.0
XI=0.0
RN=FLOAT(NR)
PSI1=0.0
PROD1=0.0
DO 1 I=2, ML
X2=X1+DX
PSI2=.1#X2
PROD2=PSI2*Y(I)
Q=Q+(PROD2+PROD1)*DX/2.0
PRCD1=PROD2
XI=X2
1 CONTINUE
Q=Q/2.0
WRITE(6, 100)M, NR, Q
FORMAT(6, 100, 10X, 10)
FORMAT(10, 10, GENERALIZED AERODYNAMIC FORCE: , //)
RETURN
END
100
101
00002650
00002660
00002670
00002680
00002690
00002700
00002710
00002720
00002730
00002740
00002750
00002760
00002770
00002780
00002790
00002800
00002810
00002820
00002830
00002840
00002850
00002860
00002870
00002880
00002900
00002910
00002920
00002930
00002940
00002950
00002960
00002970
00002980
00002990
00003000

```

LIST OF REFERENCES

1. Grumman Research Dept., Rept. no. Re-488, Self Excited Super Turbulence-The Whistler Nozzle, Hill and Greene, October 1974.
2. Grumman Research Dept., Effects of Initial Conditions on Mixing Rates of Turbulent Jets, Hill and Jenkins, To Be Published.
3. Rockwell International, NP75H-129, A Study of Potential Techniques for Increasing Jet Entrainment Rates In Ejector Augmenters, Schum, E.F., October 1974.
4. ARL 75-0224, Thrust Augmenting Ejectors, Viets, H., June 1975.
5. Crow and Champagne, "Orderly Structure in Jet Turbulence", Jo. of Fluid Mechanics, Vol 48, 1971.
6. Bevilacqua and Lykoudis, "The Mechanism of Entrainment", AIAA Jo., Volume 9, August, 1971.
7. Ricou and Spalding, "Measurement of Entrainment by Axisymmetric Turbulent Jets", Jo. of Fluid Mechanics, Volume 11, 1971.
8. AFFDL-TR-73-55, Advanced Ejector Thrust Augmentation Study-Mass Entrainment Of Axisymmetric And Rectangular Free Jets, Peschke, W., April 1973.
9. AEDC-TR-71-36, Free Turbulent Mixing: A Critical Evaluation Of Theory And Experiment, Harsha, P.T., February 1971.
10. Weinger, S.D., "The Effects of Sound on a Reattaching

Jet at Low Reynolds Numbers", Fluid Amplification Symposium, Volume 4, October, 1965.

11. ASME Power Test Codes, Supplement, Chapter 4, Part 5, Flow Measurement, Instruments and Apparatus, February 1959.
12. Bell, J.K., Theoretical Investigation of the Flutter Characteristics of Supersonic Cascades with Subsonic Leading - Edge Locus, Naval Post Graduate School Thesis, June, 1975.
13. Brix, C.W., Jr., A Study of Supersonic Flow Past Vibrating Shells and Cascades, Naval Post Graduate School Thesis, June, 1973.
14. Zierep, Jurgen, "Auftrieb und Widerstand Langeringflugel in Uberschallstromung", Wissenschaftliche Gesellschaft fur Luftfahrt e. V., January 1957.
15. ARL report No. 74-0113, "Development of a Time Dependent Nozzle", Viets, H., July 1974.
16. Platzer, "Wind Tunnel Interference on Oscillating Airfoils in Low Supersonic Flow" Acta Mechanica, Vol. 16, pages 115-126, 1973.

END
8-76